3-26-2015

Ionizing and Non-ionizing Radiation Effects in Thin Layer Hexagonal Boron Nitride

Brian L. Barnett

IONIZING AND NON-IONIZING RADIATION EFFECTS IN THIN LAYER HEXAGONAL BORON NITRIDE

THESIS

Brian L. Barnett, Major, USA

AFIT-ENP-MS-15-M-099

DEPARTMENT OF THE AIR FORCE
AIR UNIVERSITY

AIR FORCE INSTITUTE OF TECHNOLOGY

Wright-Patterson Air Force Base, Ohio

AFIT-ENP-MS-15-M-099

IONIZING AND NON-IONIZING RADIATION EFFECTS IN THIN LAYER HEXAGONAL BORON NITRIDE

THESIS

Presented to the Faculty

Department of Engineering Physics

Graduate School of Engineering and Management

Air Force Institute of Technology

Air University

Air Education and Training Command

In Partial Fulfillment of the Requirements for the

Degree of Master of Science in Nuclear Engineering

Brian L. Barnett, BS

Major, USA

March 2015

AFIT-ENP-MS-15-M-099

IONIZING AND NON-IONIZING RADIATION EFFECTS IN THIN LAYER HEXAGONAL BORON NITRIDE

Brian L. Barnett, BS

Major, USA

Committee Membership:

Dr. J. C. Petrosky
Chair

Dr. S. A. Francis
Member

Dr. B. J. Singleton
Member

Abstract

The radiation response of 14nm h-BN/Si metal insulator semiconductor (MIS) devices was investigated using current-voltage and capacitance-voltage measurements indicating Frenkel-Poole (FP) and Fowler-Nordheim tunneling (FNT) are the primary current mechanisms before and after irradiation. The data were fit to a composite model of FP and FNT currents.

Irradiations to 33.1, 99.3, and 331 krad(Si) from a cobalt-60 source causes a negative voltage shift to the current-voltage measurements of -0.14, -0.45, and -0.46 V respectively. The negative shift indicates radiation induced production of positive space charge at the h-BN/Si interface. No device characteristic changes were observed following gamma irradiation. Fitting the model to data collected after neutron irradiation at a fluence of 3.76×10^{15} n/cm^2 indicated no change in the barrier potential for the linear FNT model and a 0.013 eV increase in the barrier potential for the FP model. There was a decrease of 0.19 eV in the tunneling potential for the non-linear FNT model. Defects generated by the neutron damage increased currents by increasing trap assisted tunneling (TAT).

Acknowledgments

I would like to express my sincere appreciation to my faculty advisor, Dr. James Petrosky, for his guidance and support throughout the course of this thesis effort. His insight and experience were certainly appreciated and invaluable. I would like to thank Dr. Michael Snure of the Air Force Research Laboratory for providing all the devices and providing valuable insight. I would also like to thank the very capable staff at the Ohio State University Research Reactor.

I especially wish to thank my wife, an amazing woman who provides me with amazing support and encouragement.

Brian L. Barnett

Table of Contents

List of Figures

Page

List of Tables

Page

Constants and Parameters

Physical Constants

Constant	Expression	Value	Units
k	Boltzmann's constant	1.38×10^{-23}	J/K
h	Planks Constant	6.626×10^{-34}	J s
q	electronic charge	1.609×10^{-19}	Coulombs
m_e	free electron mass	9.11×10^{-31}	Kg
ε_o	permittivity of free space	8.854×10^{-12}	F/m
h	Planck's constant	6.625×10^{-34}	J*s

Material Parameters

Parameter	Expression	Value	Units	Reference
e_r	Permittivity of h-BN	$2.97\varepsilon_o$	F/m	
ϕ_{BN}	BN Band Gap	3.6-7.1	eV	[5]
m^*_{BN}	effective mass of electron in h-BN	$0.26\,m_e$	kg	[5]
σ_o	conductivity of h-BN	1.2084×10^{-13}	Ω^{-1} cm^{-1}	
ρ	Density of h-BN	2.33	g/cm^3	[7]

MIS parameters

Parameter	Description	Value	Units
A	Contact area	785.4×10^{-9}	m^2
d	h-BN Thickness	14×10^{-9}	M

IONIZING AND NON-IONIZING RADIATION EFFECTS IN THIN LAYER HEXAGONAL BORON NITRIDE

I. Introduction

Radiation hardening of electronics is a complex and important challenge. Expansion of operations in space have resulted in new standards, demand for innovative ideas, more robust technology, and better performance of electronic devices and systems that must operate in a radiation harsh environment. Graphene is an emerging two dimensional (2D) material for electronic devices due to its potential for use in high performance electronics. Graphene's sensitivity to environmental effects requires the use insulator and passivation layers to maintain performance, but options are limited. Hexagonal boron nitride (h-BN) is one candidate for use with graphene-based electronic systems because it has the same lattice structure as graphene, is an insulator, and is known to form on graphene surfaces. h-BN also has superior material and electrical properties as compared to insulators such as SiO_2 or Al_2O_3. Understanding the effects of radiation on h-BN will allow for a better understanding of the performance of devices when incorporating it into novel electronic systems.

1.1 Background

h-BN can be grown atomically to ~7-14 monolayers from initial estimates using atomic layer deposition (ALD). It is expected to be radiation tolerant, due in part to it being a 2D material presenting a small volume for radiation deposition and also due to its low displacement damage cross section as compared to conventional insulating materials. A 14 nm thick h-BN layer is achievable for practical electronics with nearly no gamma

attenuation or absorption due to the low probability of gamma interactions. The greatest effect of high doses of ionizing radiation will likely be charge formation at the interface between the h-BN and substrate. In this region there is a high probability for charge traps due to the lattice mismatch between the h-BN and substrate (*e.g.* cubic Si). Non-ionizing radiation (such as high energy neutrons and protons) typically leads to dislocation damage, which will add crystal defects, increasing the potential for charge trapping following irradiation. h-BN has an added sensitivity to neutron radiation damage because of the extremely high neutron cross section of boron of 3840 b[1], and is a focus of this research [1].

h-BN is a wide band gap, III-V compound that is both physically and chemically stable. h-BN is formed from alternating boron and nitrogen atoms in a honeycomb arrangement consisting of sp^2-bonded two-dimensional layers. Within each layer, boron and nitrogen atoms are bound by strong covalent bonds, whereas the individual layers are held together by weak van der Waals forces [2]. The typical thickness of a monolayer of h-BN is ~2-5 layers of 1.03-2.0 nm (0.40-0.565 nm per monolayer) as a result of chemical vapor deposition (CVD) growth [2]. Additionally, there is a strongly disordered interface layer 3-5 nm thick when it is in contact with Si. This layer contains a high concentration of dangling bonds from the large lattice mismatch between h-BN and Si [3].

h-BN has a band gap that ranges from 3.6-7.1 eV, which makes it an insulator. It has been proposed as a companion insulating material for graphene devices because it

---

[1] 1 b = 10^{-28} m^2

shares the same structure as graphene and has only a 1.7% lattice mismatch [4]. This makes it an ideal dielectric material for graphene based devices [5]. The permittivity of h-BN has a range of values depending on material processing and orientation of the crystal structure in relation to the conduction path. For h-BN at room temperature created by an atomic layer deposition (ALD) process, the permittivity ranges from 2.8, parallel to the conduction path, and 4.94, perpendicular to the conduction path [6].

Boron Nitride Devices Studied In This Research

The devices under study in this research were metal insulator semiconductor (MIS) based on a Ti/Au/h-BN/Si/Ti/Au heterostructures. The architecture is shown in Figure 1. The h-BN was deposited using ALD on top of a boron doped Si (100) substrate [7]. The Ti/Au contacts were deposited using ALD on both the top and bottom of the h-BN and Si substrate. The contact thickness was determined by growth time as 3200 Å. The Si substrate was 500 μm and the h-BN was 14 nm thick, as determined by growth time and confirmed by capacitance measurements in this research. The BN layer is made of h-BN crystals between 2-6 nm. The thickness of the h-BN crystals was measured using x-ray diffraction (XRD) [7].

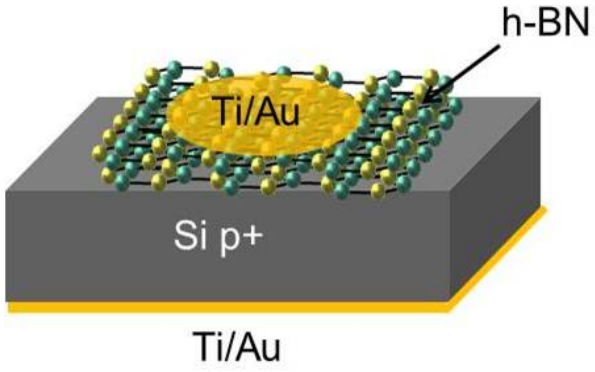

Figure 1. h-BN/ Si MIS device physical structure.

The h-BN/ Si MIS flat band diagram is shown in Figure 2. The band gap (E_g) of h-BN is depicted as 5.97 eV but can range from 3.6-7.1 eV depending on the method and quality of the BN fabrication [5]. The work function (Φ_M) of Ti/Au is 4.8 eV and the band gap (E_g) of Si is 1.12 eV [8]. The calculated flat band (V_{FB}) is -0.289 eV and the electron affinity of h-BN (X_{BN}) and Si (X) is 2.971 eV and 4.05 eV respectively.

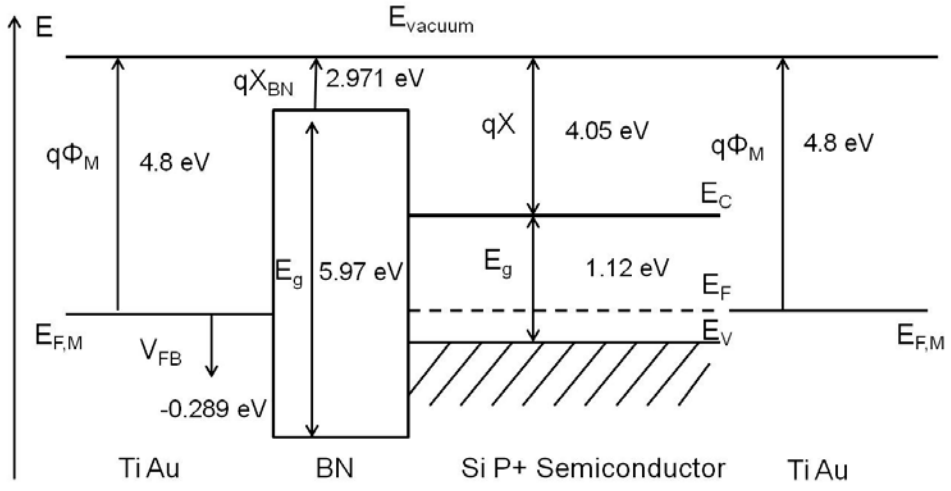

Figure 2. h-BN/Si p+ MIS flat band diagram.

Current-voltage (*I*-*V*) and capacitance-voltage (*C*-*V*) characteristics provide information regarding electrical performance changes of the MIS device following use and radiation damage.

The focus of this research was to identify how h-BN MIS devices will perform after being exposed to ionizing and non-ionizing radiation. Another important aspect was also to identify the relevant current modes that dominate current through the devices, and use them to quantify the device electrical behavior.

1.2 Research Justification

The radiation performance of h-BN is not well understood because it is a relatively new material for use in electrical devices, and the material properties vary with quality and fabrication. Determining the radiation response of h-BN MIS devices will enable material scientists to design new generations of graphene based electronics that will be radiation resistant and maintain graphene's electrical properties. Furthermore, determining the radiation response may enable development of a technology that can operate reliably in harsh radiation environments such as space and in nuclear reactors.

Problem Statement

The primary focus of this research was the radiation response of h-BN due to incident ionizing and non-ionizing radiation. It required analyses to determine the current, capacitance and voltage dependent response of the device, and applying theory to determine the cause of the changes in the electrical performance after ionizing and non-ionizing radiation.

Hypotheses

It can be demonstrated using *I-V* and *C-V* measurements that the h-BN MIS will exhibit changes in electrical performance due to both ionizing and non-ionizing irradiation. The *I-V* measurements will reveal the contributions of Frenkel-Poole (FP) emission, Fowler-Nordheim tunneling (FNT), and Schottky emissions.

Neutron irradiation will increase the transverse current due to displacement damage. Analysis of the changes in the current model using FP emission and FNT will identify the mechanisms responsible for the increased transverse currents.

1.3 Research Objectives

1. Determine the dominant current mechanism for h-BN/Si MIS devices.

2. Design, construct and test experiments that enable gamma and neutron irradiations, but will also prevent device degradation due to electrical sensitivities (charge buildup, electrostatic effects).

3. Characterize MIS devices as a function of gamma and neutron irradiation using current and capacitance measurements.

4. Use *I-V* and *C-V* measurements and modeling to determine the cause of the changes in current and capacitance.

1.4 Scope

This research is limited in the determination of the electrical response (current, capacitance and voltage) in the h-BN/Si heterojunction and between -1 to 1 V. Current and capacitance is studied before and after gamma and neutron irradiations.

1.5 Methodology

Theoretical development, modeling, and experimental measurements were used in this effort. Current models for MIS contacts were used in the development of the current model. FP emission and FNT was modeled using measured data [5, 9]. The contribution of each current model was determined using accepted physical constants, nominal values for contact dimension, and order-of-magnitude scaling for calculating parameters such as doping density. The current and capacitance before and after gamma and neutron irradiation were measured as a function of applied voltage. The model parameters were then varied to find the best fit to the *I-V* data and suggest causes to the changes in current after irradiation.

1.6 Assumptions/Limitations

The FP and FNT currents will dominate the current in high electric field regions, and the primary model will account for changes in the model parameters from irradiation. It is also assumed that the gamma irradiation that occurs during neutron irradiation in the reactor will not contribute significantly to the creation of defects because of the low non-ionizing energy loss (NIEL) of gamma rays in h-BN and Si.

1.7 Sequence of Presentation

This thesis is separated into five chapters. The first chapter has provided an introduction to the device design and background information. Chapter two presents the results of literature search and details in the current models. Chapter three presents the experimental setup and procedure for both gamma and neutron irradiations. Chapter four

describes the results of the experiments. Chapter five contains the conclusion and recommendations for future work.

II. Research Review and Model Development

2.1 Chapter Overview

A review of recent h-BN MIS research identified three leakage models that could account for current flow within the MIS devices. The current models for MIS devices include Schottky emission, Frenkel-Poole emission (FP), and Fowler-Nordheim tunneling (FNT). The most likely models that account for the current would be the FP and FNT. The Schottky emission is eliminated from consideration because the h-BN does not form an ohmic contact with Ti/Au [7] and the local electric field strength is high enough to allow FNT to dominate in the positive voltage region [8].

2.2 Model Development

In this section the device structure is presented and possible current paths are proposed. The available current paths in this structure are shown in Figure 3; 1) along the surface of the h-BN until it finds a preferential path through the Si ; 2) through the h-BN and then along the interface of the h-BN/Si interface; 3) through both h-BN and the h-BN/Si interface in a direct manner.

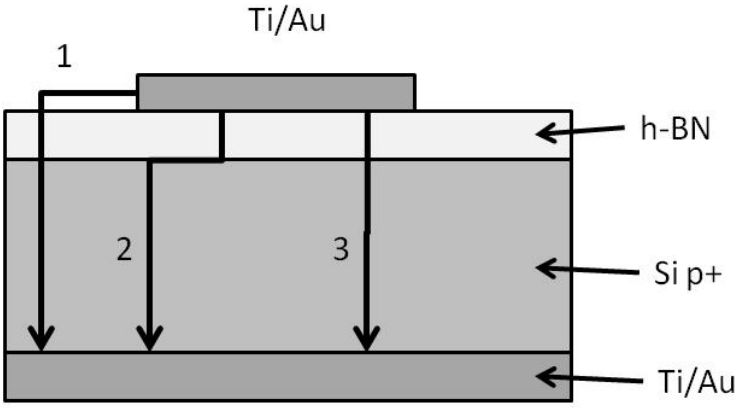

Figure 3. Current path diagram.

Each current path can be modeled as an equivalent circuit as shown in Figure 4. Current path 3 corresponds to the FNT and FP emissions for positive and negative voltage regions respectively. Paths 1 and 2 include parasitic resistances as the applied potential increases and allows for additional current paths [9].

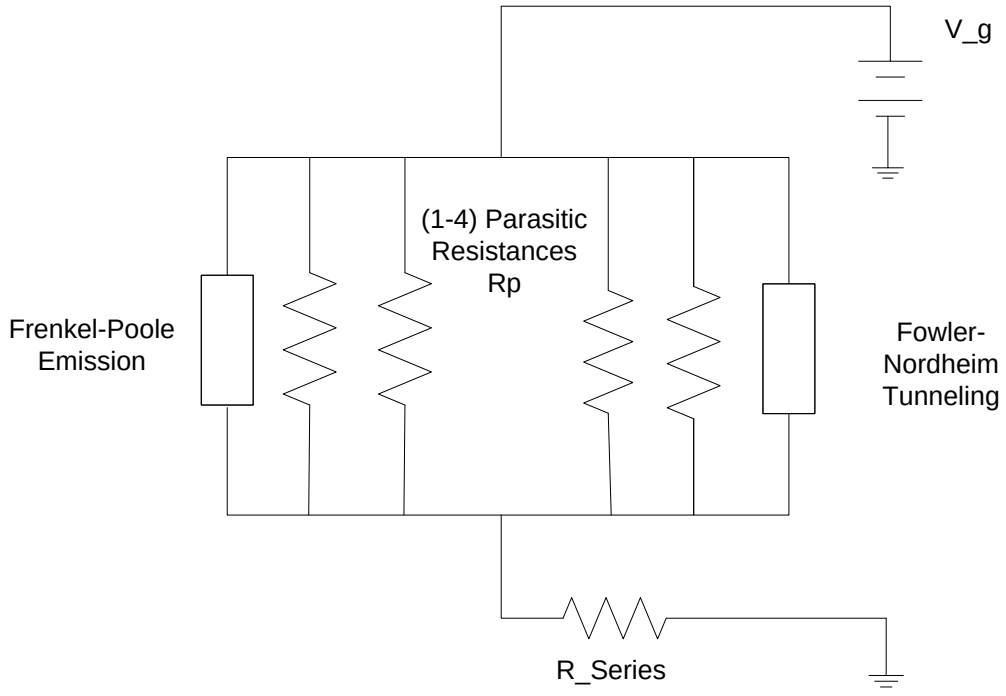

Figure 4. Equivalent circuits for proposed current paths in h-BN MIS devices.

The circuit diagram for capacitance is depicted in Figure 5. The capacitance of the h-BN, labeled *C_BN*, is in series with the capacitance of the silicon, *C_Si*, with corresponding resistivity in parallel with each capacitance, *R_BN* and *R_Si*, which correspond to leakage paths.

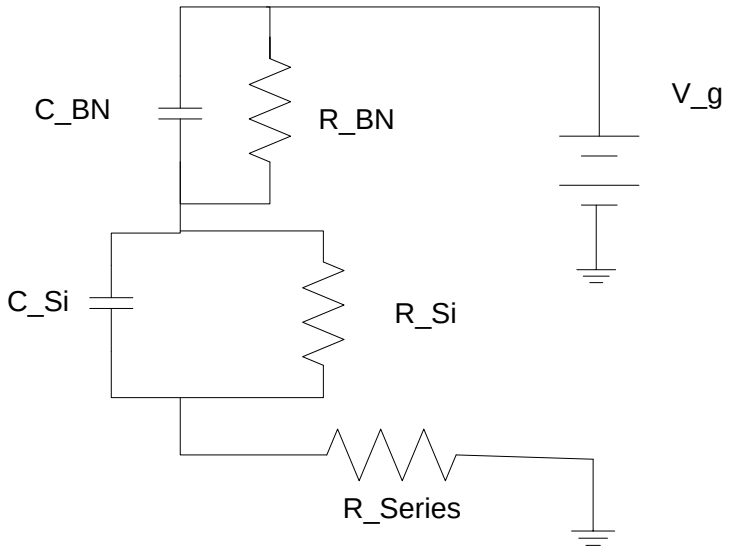

Figure 5. Equivalent circuit for capacitance in the h-BN MIS device.

Schottky emission, represented by path 1 in Figure 6, is a thermal induced flow of charge over a potential barrier. Frenkel-Poole emission is a method by which an insulator can conduct current. Since the electrons are in loosely bound states, thermal fluctuations can give them enough energy to move them into the conduction band. When an electric field is applied, the electrons do not require as much thermal energy to move into the conduction band. Path 2 in Figure 6 shows the FP emission under an electric field. FNT is a direct tunneling method where the electron under a strong enough electric field has enough energy to tunnel to the conduction band. It is represented by path 3 in Figure 6.

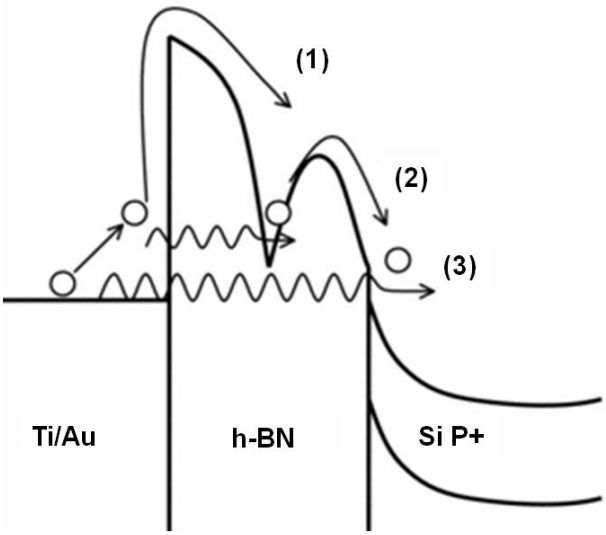

Figure 6. Energy band model of 1) Schottky emission, 2) Frenkel–Poole emission and 3) Fowler–Nordheim tunneling. Reproduced from [10].

2.3 Frenkel-Poole Emission (FP) Model

The current-voltage relationship for Frenkel-Poole emission is $\ln(I/V) \propto 1/V^2$.

The current-voltage relationship including FP emission for the h-BN MIS structure is shown in Equation 2.1 [9].

$$I(V) = A\sigma_o \frac{V}{d} e^{\left[\frac{-q}{kT}\left(\Phi_{FP} - \sqrt{\frac{qV}{\pi\varepsilon_o\varepsilon_r d}}\right)\right]} \tag{2.1}$$

In (2.1), A is the area of the contact, σ_o is the conductivity of h-BN, V is the applied potential, d is the thickness of the h-BN, T is the temperature, Φ_{FP} is the barrier potential for the conduction band, and ε_r is the permittivity of h-BN.

2.4 Fowler-Nordheim Tunneling (FNT) Model

The current-voltage relationship for FNT is $\ln(I/V^2) \propto 1/V$. The current-voltage relationship for the h-BN MIS including FNT is shown in Equation 2.2 [5].

$$I(V) = \frac{A_{eff} q^3 m V^2}{8\pi h \phi_B d^2 m^*} e^{\left[\frac{-8\pi\sqrt{m^*}\phi_B^{3/2} d}{3hqV}\right]} \tag{2.2}$$

In (2.2), A_{eff} is the area of the contact, m is the electron mass, m^* is the effective mass of an electron in h-BN, ϕ_B is the barrier potential for tunneling, and d is the h-BN thickness.

Under a weak electric field, (2.2) can be simplified to a linear relationship as in (2.3) [5].

$$I(V) = \frac{A_{eff}\sqrt{m\phi_B} q^2 V}{h^2 d} e^{\left[\frac{-4\pi\sqrt{m\phi_B} d}{h}\right]} \tag{2.3}$$

Modeling and Fitting Current Equations

The expected ranges of the values of the fitting parameters for the FP and FNT models for h-BN MIS are given in Table 1, and the independent variable values are given in Table 2.

Table 1. Expected range of values of model fitting parameters.

Parameter	Range of Values	Units
ϕ_B	1.1-1.6	eV
m^* [5]	0.26 m	*kg*
R_P [11]	~1-50	GΩ
ϕ_{FP}	0.1-0.2	eV

Table 2.Values of independent variables.

Independent Variable	Values	Units
A	785.4×10^{-9}	m^2
N	10^{18}	cm^{-3}
σ_0	1.21×10^{-13}	$\Omega^{-1}\ m^{-1}$
T	300	K
D	14×10^{-9}	m
ε_r	2.97	

The flat band potential for the h-BN MIS is calculated using (2.4) and (2.5) [12].

$$V_{FB} = V_T - 2\phi_F - \frac{\sqrt{4\varepsilon_s qN\phi_F}}{C_{ox}} \tag{2.4}$$

$$\varepsilon_s(N) = 11.7 + \frac{1.5\times10^{-16}N}{105.3 - 4.9469\times10^{-5}N^{1/3} - 3.283\times10^{-18}N} \tag{2.5}$$

In (2.4) and (2.5), N is the doping density of the Si substrate in cm^{-3}. Equation (2.5) is an empirical equation that calculates the permittivity of Si under different doping densities [12]. Combining (2.4) and (2.5), and solving for N, one gets a doping density of $10^{18}\ cm^{-3}$.

Table 3.Values used for calculation of V_{FB}.

Variable	Values	Units
ϕ_F	1.12	eV
V_T	4.8	V
C_{ox}	1.47×10^{-12}	F
V_{FB}	0.28	V

Using the measured capacitance value of 1.47 nF and the doping density of 10^{18} cm^{-3} , the permittivity of the h-BN can be calculated using (2.6).

$$\varepsilon_{ox} = \frac{t_{ox} C_{eff}}{A_{eff}} \tag{2.6}$$

The permittivity of h-BN is calculated as 2.97, which is close to the reported value of polycrystalline BN [1].

III. Equipment and Procedures

3.1 Primary Experimental Equipment Descriptions

Probe Station

The Signatone probe station has four stabilized probe arms that are capable of connecting to a Keithley 4200 semiconductor characterization system (SCS), which has three current/voltage source measurement units (SMUs) and two capacitance SMUs. The probe station uses extremely low resistive probe tips and wires to make contact with electronics. The probe arms are stabilized to a floating platform through a vacuum seal. The electronic devices are also secured to the bottom chuck through this vacuum.

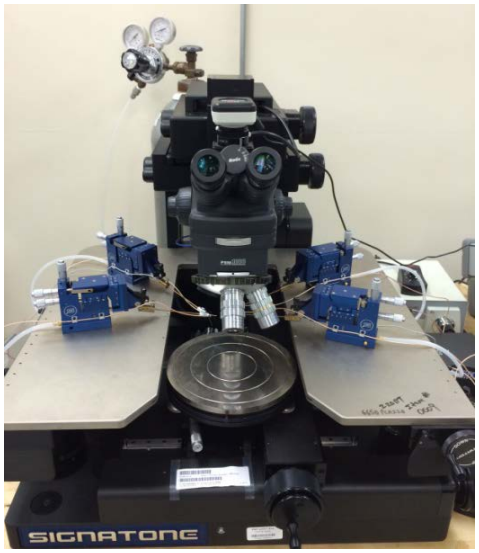

Figure 7. Signatone probe station with Keithley 4200 semiconductor characterization system.

The Keithley 4200 has an operating range of +/-200 V with a built-in voltage accuracy of 0.02 % of the measured value. It has a voltage resolution of 0.1 to 100 μV.

The current capabilities range from +/- 100 mA with a built-in current accuracy of 0.04% of the measured value. It has a current resolution of 0.1 to 100 pA [13]. The Keithley 4200 stores all measurements in a table format and exports the data file to an Excel workbook.

OSURR Cobalt-60 Gamma Irradiator

The gamma irradiation experiments took place at the Ohio State University Research Reactor (OSURR) cobalt-60 gamma irradiator. The gamma irradiator is a cobalt-60 source surrounded by at 10 ft deep pool of water. The cobalt-60 source emits 1173 keV and 1333 keV gamma ray photons. The pool provides shielding from the source. For all experiments, the devices were irradiated in aluminum foil pouches and connected to a grounding wire to prevent charge collection in the devices, which could have potentially damaged them. The devices were lowered into the 6" experiment tube to the peak dose-rate location ~9" from the bottom of the tube. The dose-rate of the cobalt-60 source on the day of irradiation was 36.9 krad/hr (H_2O), which is equivalent to 33.1 krad/hr (Si).

The Ohio State University Research Reactor (OSURR)

The neutron irradiations took place at the OSURR, which is an enriched ^{235}U reactor surrounded by a 20 ft deep pool of water. The pool provides cooling, neutron moderation, and radiation shielding. The auxiliary irradiation facility (AIF) was used for the irradiation of the devices, and is shown in Figure 8.

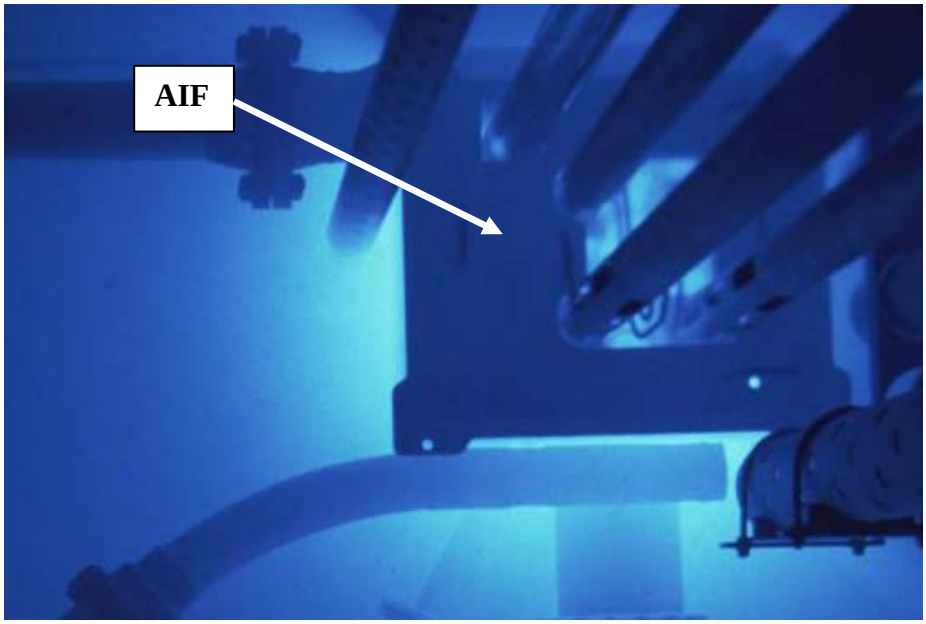

Figure 8. Photograph of the OSU research reactor with AIF location [14].

As with the gamma radiation experiments, devices being irradiated in the AIF were placed into aluminum foil pouches and connected to a grounding wire to prevent charge buildup. The grounding wire was attached to the AIF experiment vessel as shown in Figure 9.

The AIF experiment vessel is made of 2024 aluminum, which will become radioactive via neutron capture in aluminum, but will be less radioactive than other types of aluminum with more copper and zinc alloys, and will be substantially less radioactive than that of the reactor. Therefore, the aluminum activation was not considered to be a significant source of gamma irradiation to the samples.

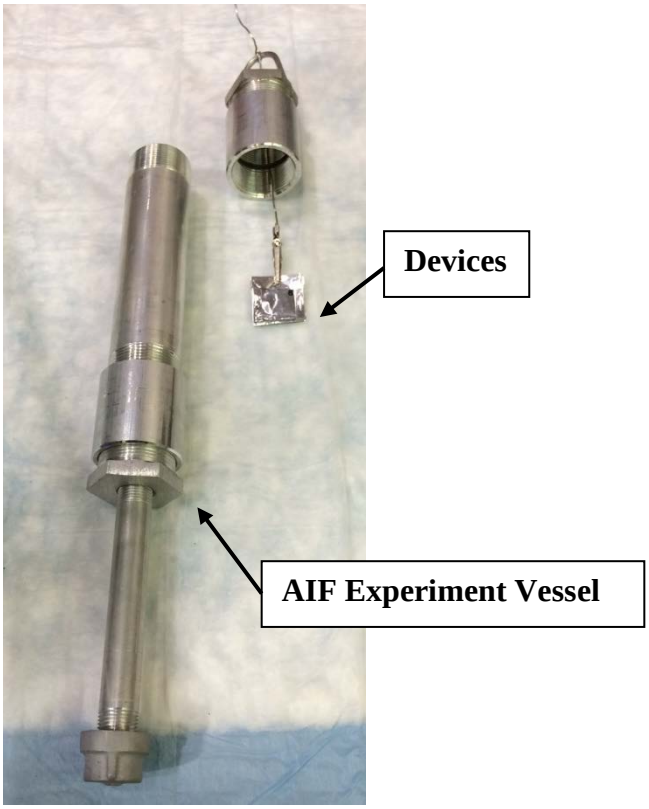

Figure 9. Experimental setup illustrating device placement inside of the experiment vessel.

3.2 Irradiation Procedures

Devices in this study were characterized prior to and following gamma and neutron irradiation using *I-V* and *C-V* measurements. The *I-V* and *C-V* data were then analyzed to identify mechanisms responsible for the observed radiation-induced changes. Special care was taken throughout all steps of pre-characterization, device preparation, and irradiation to ensure there was no electrostatic discharge (ESD) or physical damage. The devices were all handled using tweezers and wearing proper ESD wrist straps.

Pre-Characterization

All pre- and post-irradiation *I-V* and *C-V* measurements were made using the same equipment, cables, and configurations. Samples were characterized prior to

irradiation to ensure the equipment would provide the required precision, as well as to establish pre-irradiation *I-V* and *C-V* measurements to compare to post-irradiation measurements.

The current dependence on voltage was measured using the Signatone probe station and the Keithley 4200 SCS. The high potential probe was put on the top contact and the bottom contact was connected to ground through the chuck holding the device and a second probe tip. The Keithley KITE program was used to record each *C-V* measurement. The applied voltage was swept from -0.5 to 0.5 V using a step function in increments of 0.01 V for a total of 101 measurements. Five to ten independent *I-V* measurements were made for each device. This was accomplished by raising the high potential probe tip after each measurement and placing it back on the contact at a different location. This procedure was repeated for each device on the chip. The same procedures used for the *I-V* measurements were used for the *C-V* measurements, but two Keithley 590 CV analyzers were connected to both the high potential probe and the low potential. Each chip had between 6-16 devices on each, for a total of 30-600 independent measurements for each chip.

Device Irradiation Procedures

The devices were put in aluminum foil packets connected to the top and bottom contacts. Each packet was connected to a grounding wire by an alligator clip at the top edge of the packet for the duration of the irradiation. The group of devices was positioned in the experiment vessels to correspond to the peak gamma or neutron flux. For the gamma irradiation, this procedure was repeated with the same devices three times with 1,

3, and 7 hour irradiations that correspond to total accumulated doses of 33.1, 99.3 and 331 krad(Si), respectively. After each irradiation, the *I-V* and *C-V* curves were measured for each device following the same procedure outlined in the pre-characterization section. Additionally, 24 hours later, the *I-V* and *C-V* measurements were repeated to identify any annealing at room temperature. For the neutron irradiations, the devices were prepared similarly to the devices used for gamma irradiations in grounded foil packets, but were placed in the AIF experiment vessel as shown in Figure 9. The position of the devices corresponds to the peak flux in the AIF irradiation chamber. The reactor was then powered to 50 kW for 1 hour, which corresponds to a total neutron fluence of 3.76×10^{15} n/cm^2. After irradiation, the devices and experiment vessel remained in place for 5 days to allow for the activation products to decay so that the devices could be safely extracted and handled for measurements. *I-V* and *C-V* curves were measured immediately after removal from the experiment vessel and after 24 hours to identify any room temperature annealing effects.

3.3 Dosimetry Methods

The flux at the bottom of the cobalt-60 6 inch irradiation tube is shown in Figure 10. The peak dose rate occurs at 8 inches from the bottom of the irradiation tube. All of the devices for all the gamma irradiations were placed at this position.

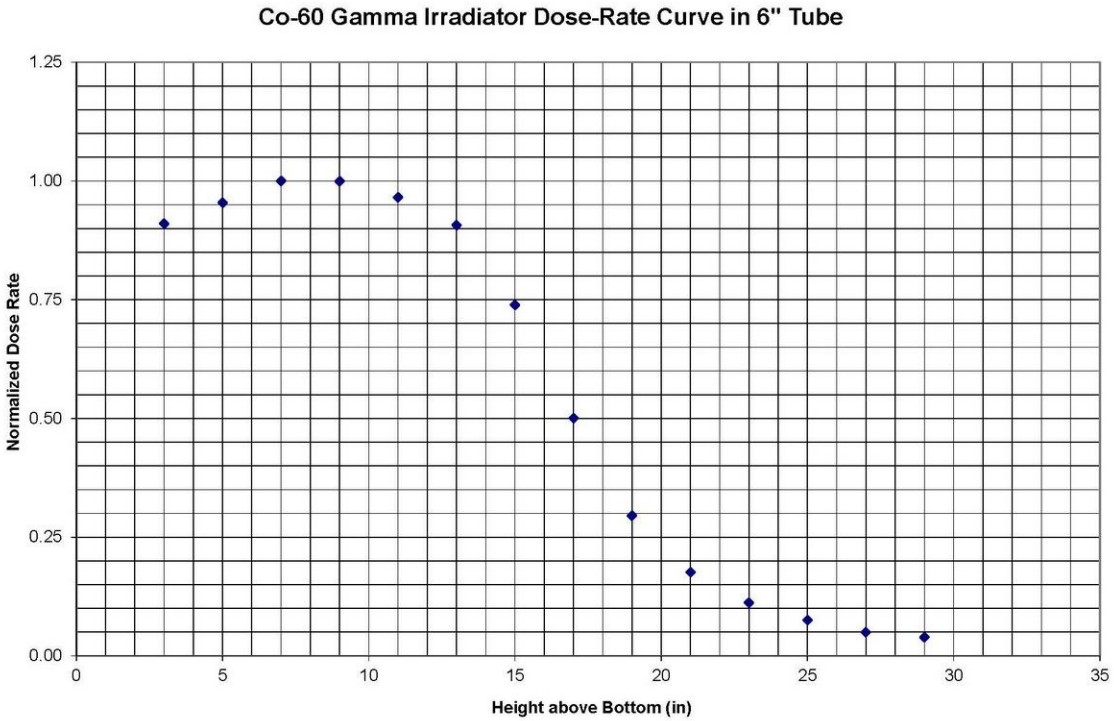

Figure 10. OSU Co-60 gamma normalized dose rate related to position [14].

The energy deposited inside of the device from gamma rays can be determined using

$$E_{Deposited} = \left(1 - \frac{I}{I_o} e^{-\rho \mu x}\right) \phi_{Gamma} t \,, \tag{3.1}$$

where I is the intensity, I_o is the initial intensity, ρ is the density of h-BN or Si, μ is the mass attenuation coefficient of h-BN or Si for the gamma ray energy, x is the thickness of the h-BN or Si region, ϕ_{Gamma} is the gamma flux of the cobalt 60 source, and t is the irradiation time.

Table 4. Table of Values for Calculated Ionizing Dose

Parameter	Silicon Substrate	h-BN
ρ	2.329 g/cm^3	2.28 g/cm^3
x	5.0×10^{-2} cm (500 µm)	1.4×10^{-6} cm (14 nm)
μ (1170 keV)	5.90×10^{-2} cm^2/g	5.047×10^{-2} cm^2/g [15]
μ (1333 keV)	5.90×10^{-2} cm^2/g	
ϕ_{Gamma}	33.1 krad (Si)	
T	1, 2, 7 hour irradiations	

The amount of energy deposited into each device during the gamma irradiation for durations of 1, 2 and 7 hours was 0.5958, 1.1916, and 4.170 krad(Si), respectively.

For neutron irradiations, the devices were placed inside the AIF at the peak flux location, which is 12 inches above the bottom of the tube, and were exposed to the neutron energy spectrum shown in Figure 11. The reactor was operated at 50 kW, while the graph depicts the spectrum at 450 kW. The neutron exposure can be scaled down 1/9th to the power of the reactor.

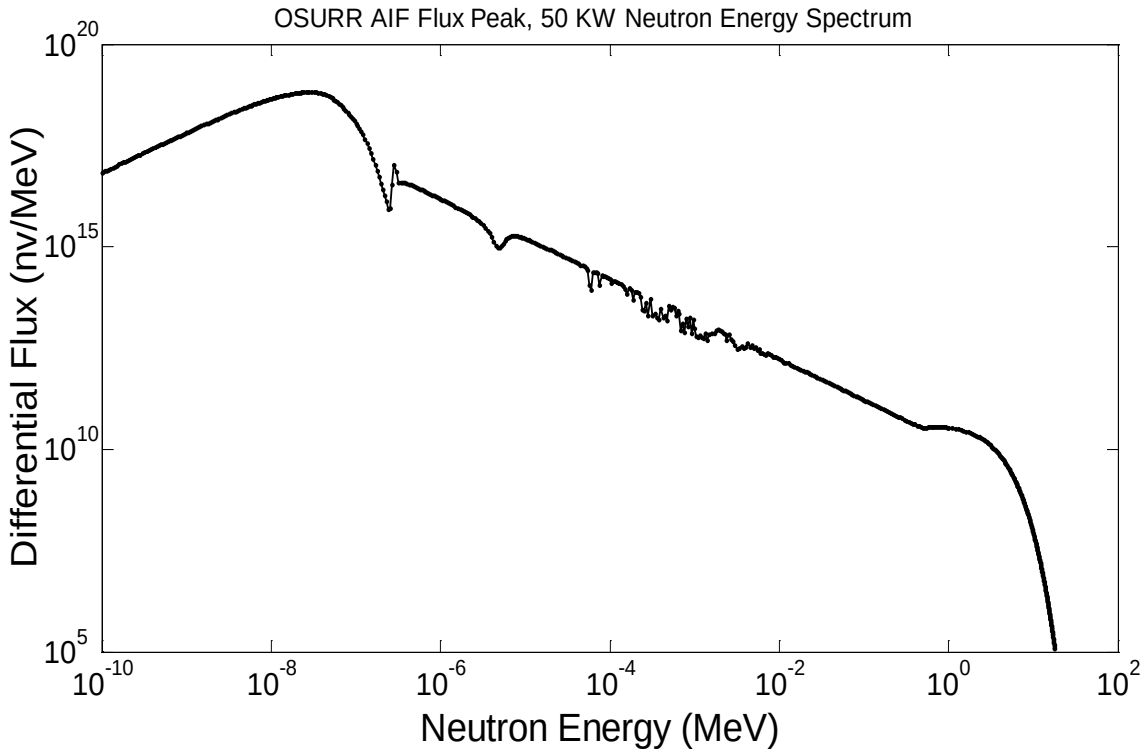

Figure 11. OSU research reactor AIF neutron fluence spectrum.

The thermal neutrons in the spectrum will interact with the ^{10}B within the h-BN and the boron doped silicon substrate to produce ^{7}Li and alpha particles. Naturally occurring boron composition is 19.8% of ^{10}B and 80.2% of ^{11}B [16].

$$^{10}B + n \longrightarrow {}^{7}Li + \alpha, \qquad 2.78 \text{ MeV } (6\%)$$
$$^{10}B + n \longrightarrow {}^{7}Li^{*} + \alpha + \gamma \ (478\text{keV}) \text{ , } 2.30 \text{ MeV } (94\%)$$

The energies of the reaction products and the range of the ^{7}Li and alpha particle are 2 and 5 μm, respectively [16]. The range of the particles in Si is much smaller than the silicon substrate thickness. Ignoring the losses for reactions at the edges of the device, all particles from the $^{10}B + n$ reaction will deposit all their energy within the device.

The number of thermal neutrons interacting with the substrate and the h-BN is shown in (3.2).

$$\text{\# of Reactions} = \phi_{n,th\_flux} t\left(1 - e^{-d\sigma N_{B-10}}\right) \tag{3.2}$$

In (3.2) $\phi_{n,th\_fluence}$ is the thermal flux, t is the time of irradiation, d is the thickness of the chip, σ is the neutron microscopic cross section for ^{10}B, and N_{B-10} is the number density of ^{10}B in the material. The total amount of thermal neutron reaction energy deposited in the device is calculated by combining the number of reactions with the average energy of the reaction products as shown in (3.3).

$$\mathrm{E}_{Th} = \text{\# of Reactions} * \frac{E_{Average}}{Reaction} \tag{3.3}$$

The contribution to the damage from fast neutrons can be calculated using the NIEL [17]. The energy deposited in the device from NIEL is shown in (3.4).

$$E_{NIEL} = 4 * NIEL_{Si} \Phi_{n,Fast} * 0.001 \tag{3.4}$$

In (3.4) $NIEL_{Si}$ is the NIEL value for Si, which is 11.65 keV/cm [17], $\Phi_{n,Fast}$ is the average integrated fast neutron flux, and the 0.001 (0.1%) is an estimation for the approximate amount of energy that results in displacement damage from NIEL in Si [17].

Combining the thermal and fast neutron energy contributions with the average energy to create a defect in Si, provides the number density of expected defects, as shown in (3.5).

$$N_{Defects} = \frac{\mathrm{E}_{Th} + E_{NIEL}}{E_{defect}} \left(\frac{1}{d_{si}}\right) \tag{3.5}$$

In (3.5), $N_{Defects}$ is the defect density, E_{defect} is the energy to create a defect in Si, 25 eV, and d_{si} is the thickness of the substrate. Table 5 shows the calculated fluences for both the cobalt-60 and the reactor for the respective irradiations.

Table 5. Calculated Dose of the Co-60 and the Reactor Fluence.

Cobalt-60			**Reactor**		
Time (minutes)	**Dose Rate (krad/hr H_2O)**	**Total Accumulated Dose (krad Si)**	**Power (kW)**	**Time (minutes)**	**Fluence (n/cm^2)**
60	37.0	33.1	50	60	3.76×10^{15}
180	37.0	99.3		Thermal	1.80×10^{15}
600	37.0	331		Fast	1.96×10^{15}

Using the fluences in Table 5, the calculated displacement damage from the 1 hour irradiation from both the thermal and fast neutrons is ~$2.0\times10^{17}\ cm^{-3}$.

IV. Analysis and Results

4.1 Chapter Overview

The combined model FP and the FNT models and parasitic resistances are used to analyze the effects of irradiation and provide the best fit to the data for both the pre- and post-irradiation *I-V* curves. The *C-V* curves provide valuable information on the material properties for both the h-BN and the silicon substrate.

4.2 Pre-characterization using *I-V* and *C-V* Measurements

The *I-V* measurements show the effective resistance, *R*, of a device according to Ohm's law, $I = V/R$. The inverse of the slope of the *I-V* curve is the effective resistance at that voltage. The Keithley 4200 has a built-in internal resistance calibration mechanism that compensates when measuring a resistance. These measurements can be used to infer the conductive properties of a material through the relationships described above. For a conventional resistor, the current increases linearly with voltage, resulting in a linear *I-V* curve, and the slope would be the resistance of the resistor. However, the h-BN device has non-linear *I-V* characteristics. Therefore, these devices could have time-dependent dielectric break down or charge breakdown, tunneling currents, and/or leakage currents. All of these measurements help characterize the dielectric quality.

The Keithley 4200 can be used to measure capacitance through the Keithley 590 *C-V* analyzer. The Keithley 590 *C-V* analyzer creates a calibrated waveform that is compared with the wave that originates from the high frequency response of the device. The combined signal is then transferred to the Keithley 4200, where the known waveform is separated from the signal and the resultant capacitance is calculated.

The high-frequency *C-V* data allow the following parameters to be extracted: oxide thickness, flat band capacitance, flat band voltage, and effective and total bulk oxide charge. Initially, the oxide thickness was used to characterize the quality and properties of the devices. Once the FP, FNT, and leakage currents were quantified, the other electrical and material properties were calculated.

The pre-irradiation *C-V* measurements of the h-BN device are shown in Figure 12. The measured effective capacitance of the device was 1.47 nF.

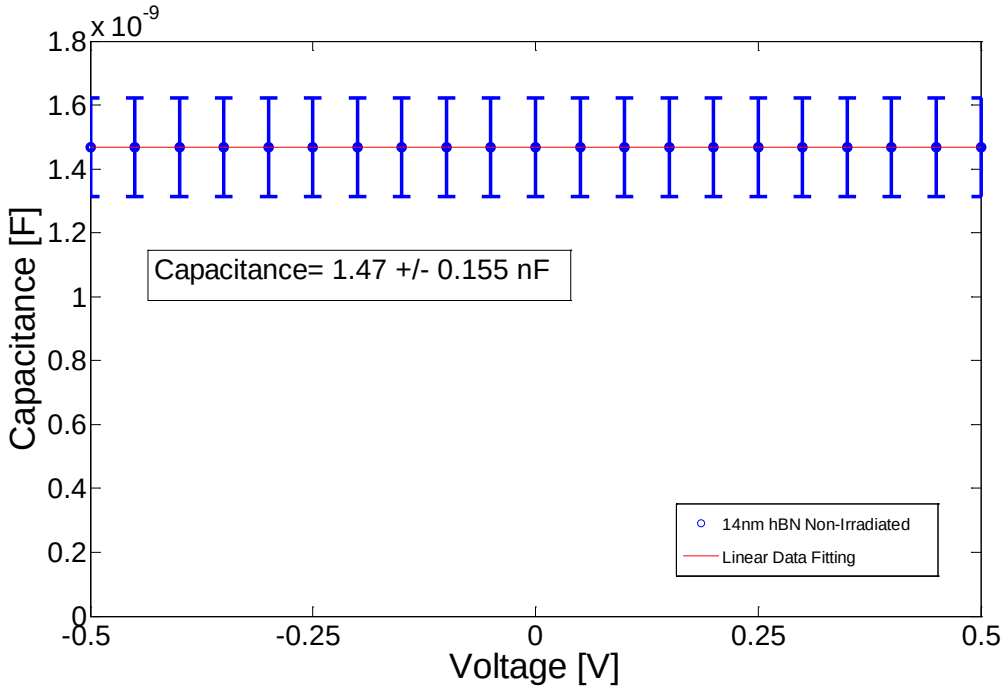

Figure 12. Capacitance as a function of voltage for h-BN, prior to irradiation.

The measured capacitance of the h-BN sample annealed at 450 K is 2.1 nF, as shown in Figure 13. The higher capacitance of the annealed h-BN device is expected because the heating in the annealing process causes the Ti/Au contacts to migrate into

both the h-BN structure and the Si substrate. This reduces the thickness of the insulating layer and linearly increases the capacitance.

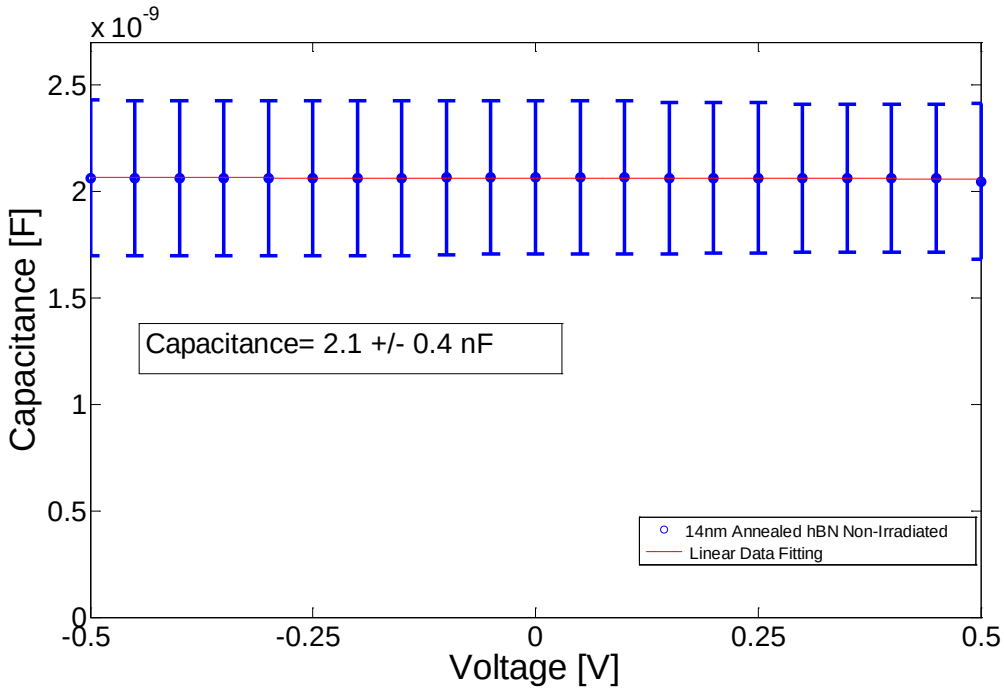

Figure 13. Capacitance as a function of voltage for h-BN annealed at 450 K, prior to irradiation.

The capacitance of the unirradiated silicon is shown in Figure 14. The measured capacitance is 237 ± 20 pF. The silicon has a measurable capacitance because the surface oxidation due to the environment forms SiO_2, resulting in an insulator that is approximately 114 nm thick.

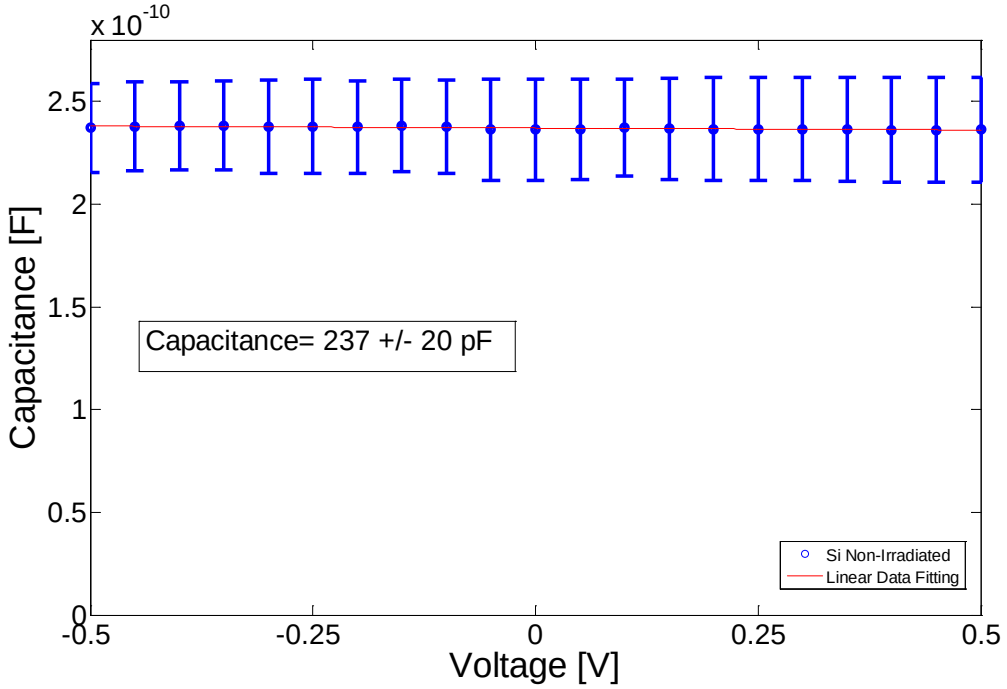

Figure 14. Capacitance as a function of voltage for p+ Si, prior to irradiation.

Figure 15 shows the *I-V* characteristics of an h-BN device prior to irradiation. The *I-V* curve has a near linear region from -0.1V to 0.5 V and a non-linear region at voltages below -0.1 V. The flat band voltage of -0.28 V shown in Figure 15 corresponds to a silicon doping density of 10^{18} cm^{-3}.

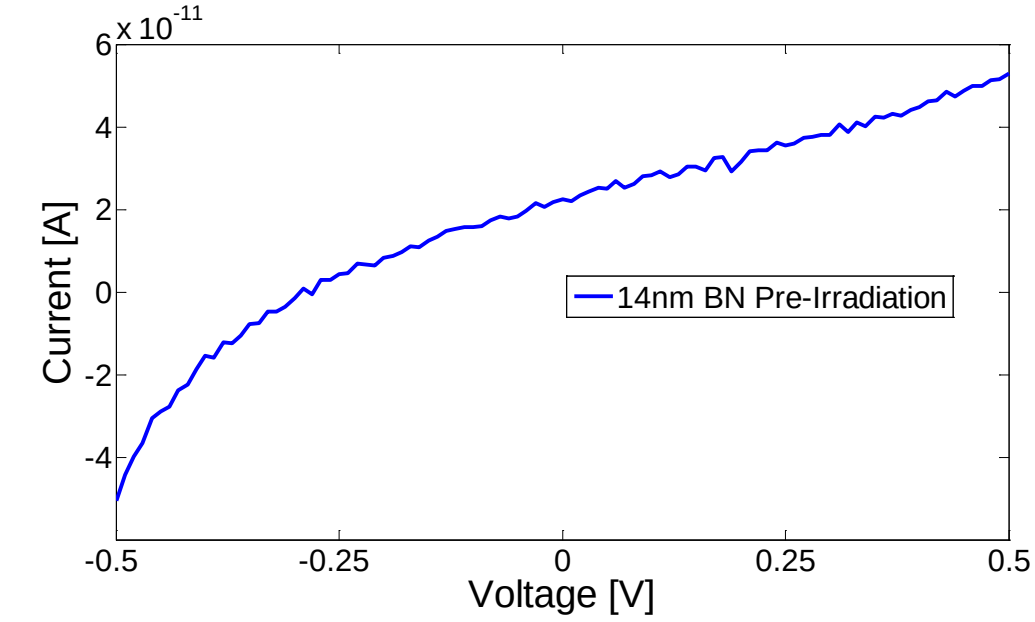

(a)

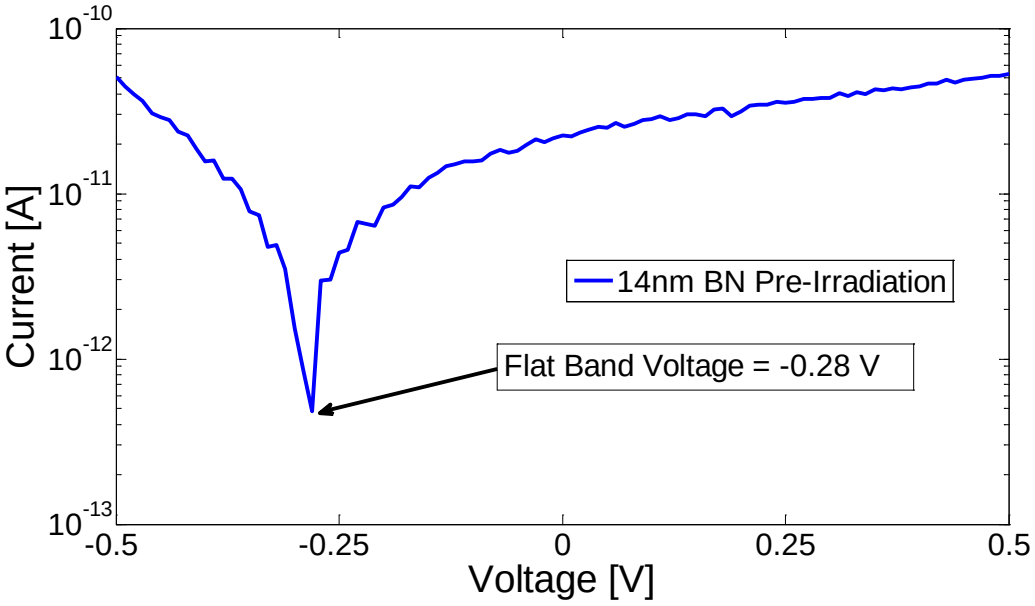

(b)

Figure 15. Current as a function of voltage for h-BN, prior to irradiation, plotted on (a) linear-linear and (b) logarithmic-linear scales.

Figure 16 provides the *I-V* data for the annealed h-BN device, prior to irradiation. The linear region covers a larger voltage range compared to the unannealed device, and has a

current magnitude of nearly one order of magnitude larger than the unannealed device. The annealing process has likely eliminated some of the defects which enabled tunneling to occur at lower positive voltages.

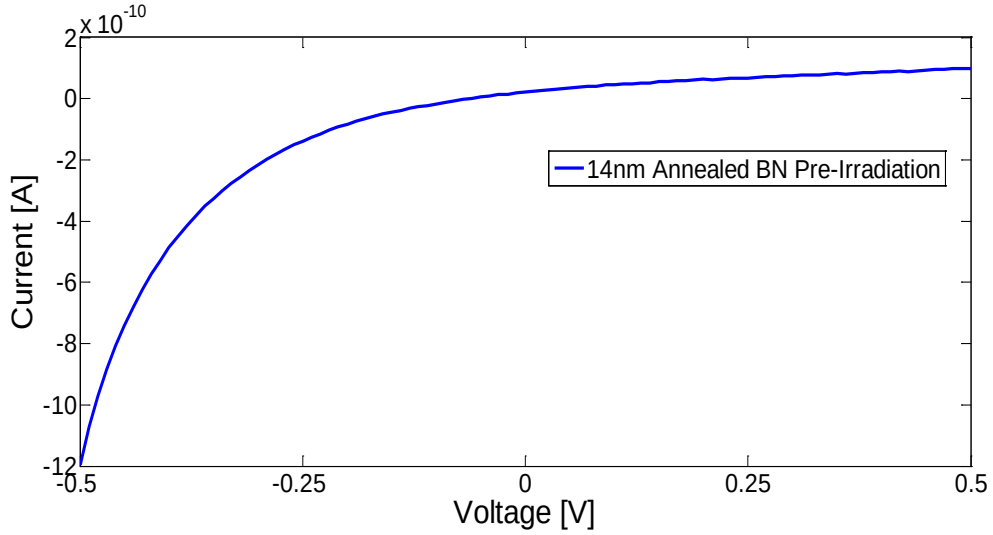

(a)

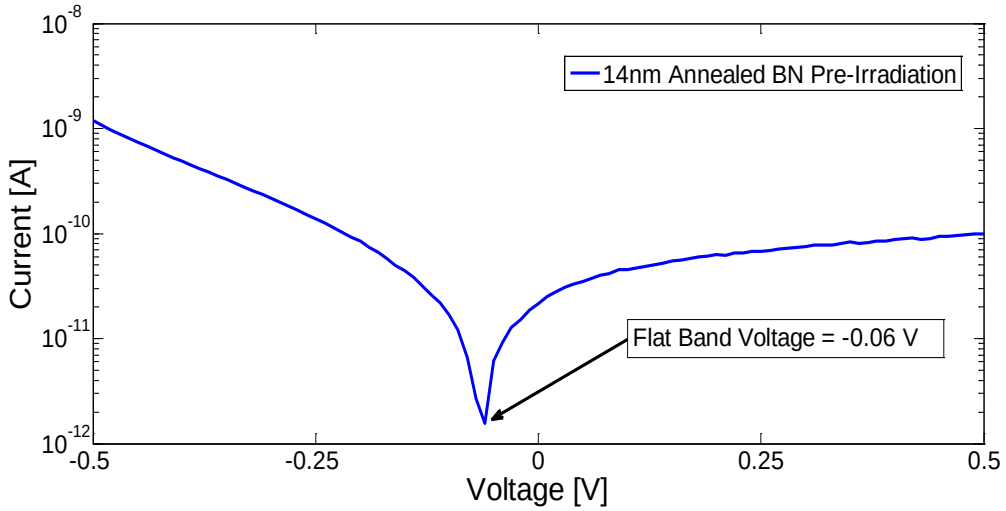

(b)

Figure 16. Current as a function of voltage for h-BN annealed at 450 K, prior to irradiation, plotted on (a) linear-linear and (b) logarithmic-linear scales.

The silicon has environmental oxidation which formed a SiO_2 layer, resembling a MOS capacitor. The approximate thickness of the Si substrate is 500 µm, with an oxide thickness of approximately 114 nm. This oxide layer results in a nonlinear region in the *I-V* curve for the Si device, as shown in Figure 17.

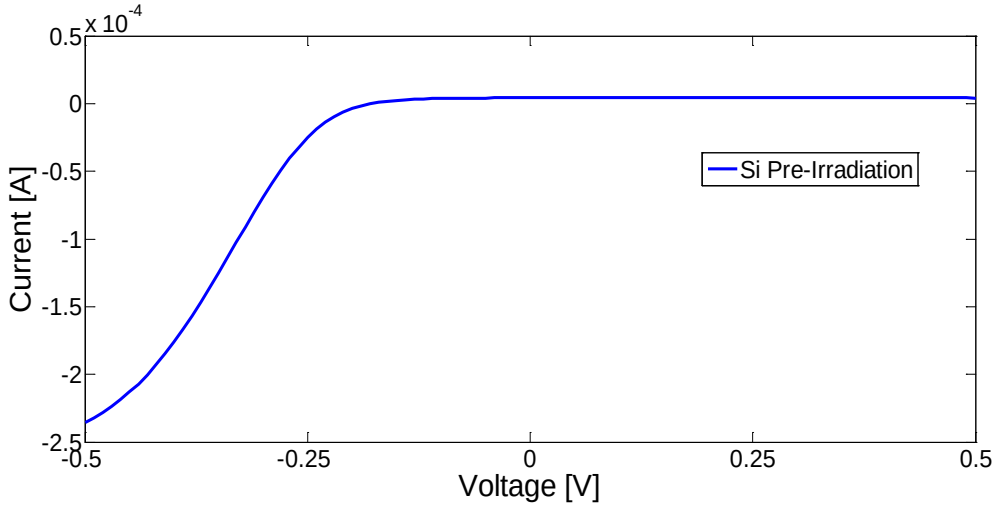

(a)

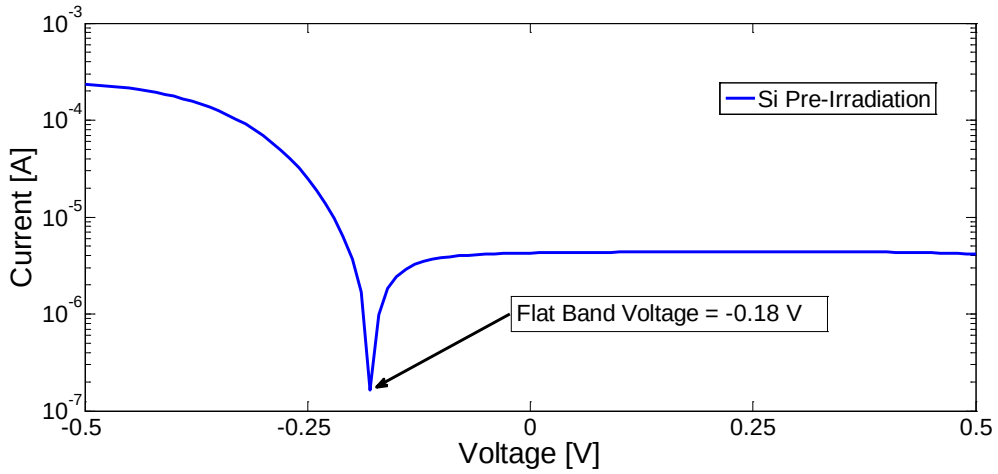

(b)

Figure 17. Current as a function of voltage for p+ Si, prior to irradiation, plotted on (a) linear-linear and (b) logarithmic-linear scales.

The combined model FP and FNT models were fitted to the pre-irradiated h-BN data, as shown in Figure 18. Every fifth measured value is shown with a single standard deviation error bar. Figure 18 shows an increasing error in the measured current in the non linear regions. The linear FNT region dominates from 0.5 V to -0.11 V and the FP model dominates from 0.11 V to -0.5 V. The higher order dependence of the FP and FNT on the applied electric field causes the FP and FNT to dominate in higher field regions.

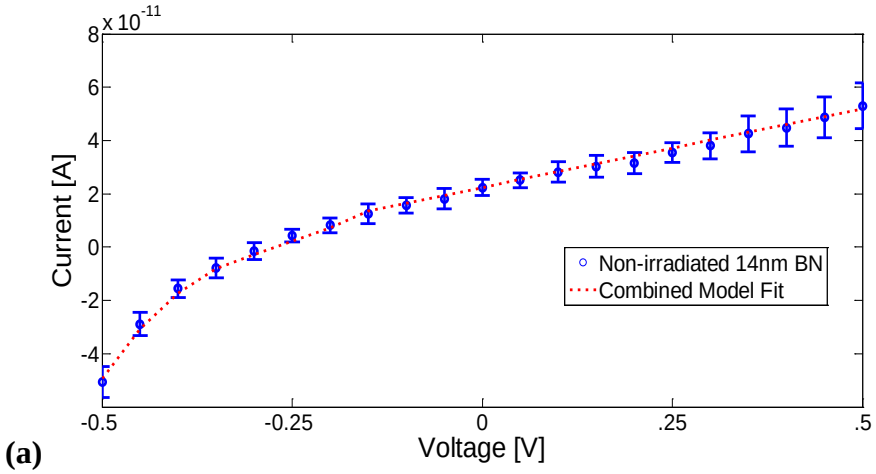

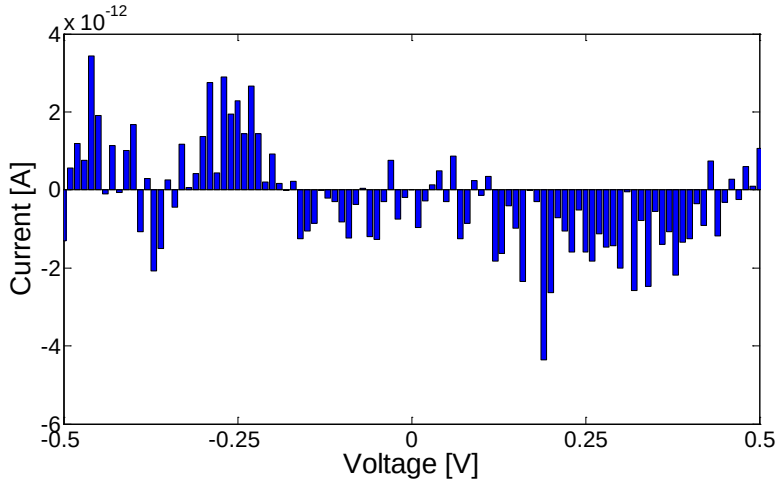

Figure 18. (a) Current as a function of voltage for 14 nm h-BN chip E, prior to irradiation, and combined FP, linear FNT, and non-linear FNT fitted models. (b) Associated residuals plot.

The residual plot between the measured and the combined model is also shown in Figure 18. The combined model fits the data within 10% of the measured value. All of the residuals are an order of magnitude smaller than the measured values. The flat band voltage is -0.28 V, and when no potential is applied, the current is 2.24×10^{-11}A. The linear FNT portion of the model has a 0.13 eV potential for tunneling. The first FP model (FP1) begins at -0.11 V and continues to -0.5 V with a barrier potential of 0.12 eV and a parasitic resistance of $2.5\times10^{10}\,\Omega$. The second FP model (FP2) begins at -0.37 V and continues in a linear combination with FP1. FP2 has a potential barrier of 0.12 eV and a parasitic resistance of $9.1\times10^{9}\ \Omega$. The non-linear FNT model was not used in this fitting because the measured positive voltage electric field was not strong enough to cause nonlinear FNT in the device. The fitting parameters for the combined model for 14 nm h-BN (chip E) are shown in Table 6.

Table 6. Fitting parameters for h-BN chip E.

Model	Parameter	Value	Units
	V_{FB}	-0.28	V
	I_{zero}	2.24×10^{-11}	A
FP 1	R_{pFP1}	2.5×10^{10}	Ω
	R_{pFP1} Begins	-0.11	V
	ϕ_{BFP1}	0.12	eV
FP 2	R_{pFP2}	9.1×10^{9}	Ω
	R_{pFP2} Begins	-0.37	V
	ϕ_{BFP2}	0.12	eV
Linear FNT	ϕ_{BLFNT}	0.13	eV
Non-linear FNT 1	R_{pFNT1}		Ω
	R_{pFNT1} Begins		V
	ϕ_{BFNT1}		eV
Non-linear FNT 2	R_{pFNT2}		Ω
	R_{pFNT2} Begins		V
	ϕ_{BFNT2}		eV

The combined FP and FNT model were fitted to the unirradiated h-BN chip D shown in Figure 19. Every fifth measured value is presented with a single standard deviation error bar. Figure 19 shows an increasing error in the measured current in the nonlinear regions and a decrease around the flat band voltage. The nonlinear FNT model dominates from 0.5 V to 0.36 V, the linear FNT region dominates from 0.36 V to -0.09 V, and the FP model dominates from -0.09 V to -0.5 V.

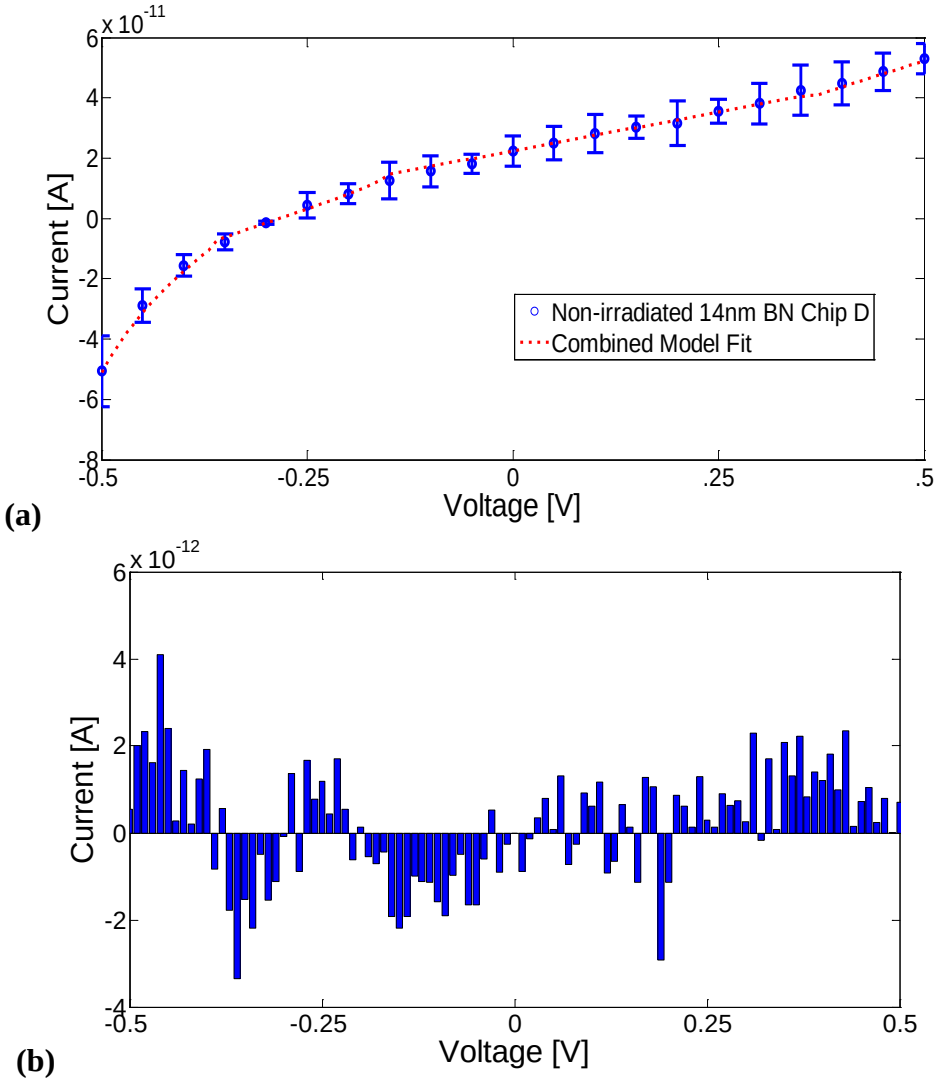

Figure 19 (a) Current as a function of voltage for 14 nm h-BN chip D, prior to irradiation, and combined FP, linear FNT, and non-linear FNT fitted models. (b) Associated residuals plot.

The residual plot between the measured and the combined model is shown in Figure 19. The combined model fits the data within 10% of the measured value. All residuals are an order of magnitude smaller than the measured values and are within the measured error ranges. The residuals show some structure and not just random fluctuations. This could result from a source of periodic noise, but does not significantly contribute to the measured values. The flat band voltage is -0.28 V and the current at 0 V is 2.2×10^{-11}A. The nonlinear FNT portion of the model shows a potential barrier of 1.31 eV for tunneling, and the linear FNT portion of the model shows a 0.131 eV potential for tunneling. The first FP model (FP1) begins at -0.09 V and continues to the -0.5 V, with a barrier potential of 0.115 eV and a parasitic resistance of $2.5\times10^{10}\,\Omega$. The second FP model (FP2) begins at -0.35 V and continues in a linear combination with FP1. FP2 has a potential barrier of 0.11 eV and a parasitic resistance of $9.1\times10^{9}\ \Omega$. The fitting parameters for the combined model for 14 nm h-BN (chip D) are shown in Table 7.

Table 7. Fitting parameters for h-BN chip D.

Model	Parameter	Value	Units
	V_{FB}	-0.28	V
	I_{zero}	2.2×10^{-11}	A
FP 1	R_{pFP1}	2.5×10^{10}	Ω
	R_{pFP1} Begins	-0.09	V
	ϕ_{BFP1}	0.115	eV
FP 2	R_{pFP2}	9.1×10^{9}	Ω
	R_{pFP2} Begins	-0.35	V
	ϕ_{BFP2}	0.11	eV
Linear FNT	ϕ_{BLFNT}	0.131	eV
Non-linear FNT 1	R_{pFNT1}	2.8×10^{10}	Ω
	R_{pFNT1} Begins	0.36	V
	ϕ_{BFNT1}	1.31	eV
Non-linear FNT 2	R_{pFNT2}		Ω
	R_{pFNT2} Begins		V
	ϕ_{BFNT2}		eV

The combined FP and FNT model were fitted to the unirradiated annealed h-BN chip F shown in Figure 20. Every fifth measured value is displayed with a single standard deviation error bar. Figure 20 shows an increasing error in the measured current in the non linear region. The linear FNT model dominates from 0.5 V to -0.13 V and the FP model dominates from -0.13 V to -0.5 V.

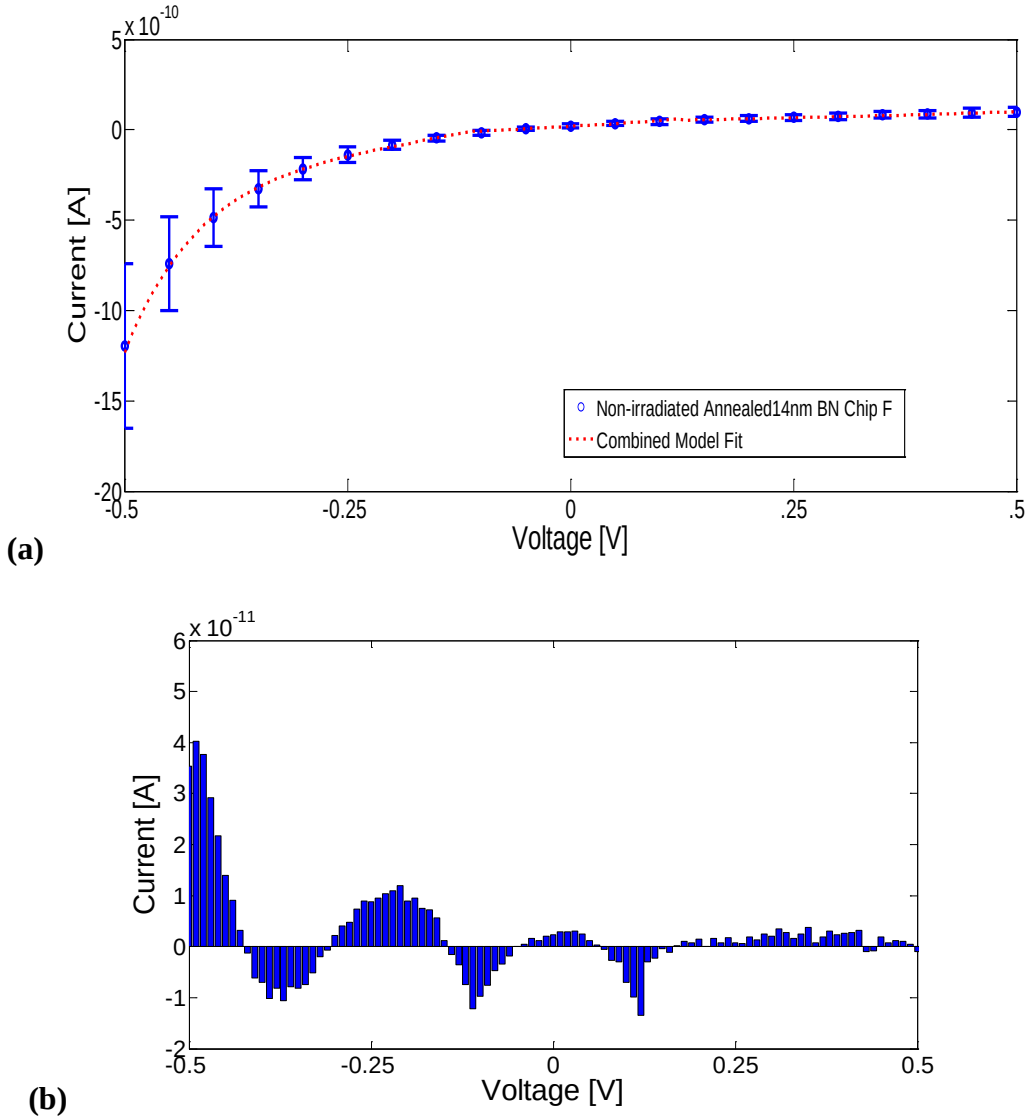

Figure 20. (a) Current as a function of voltage for h-BN chip F annealed at 450 K, prior to irradiation, and combined FP, linear FNT, and non-linear FNT fitted models. (b) Associated residuals plot.

The residual plot between the measured and the combined model is shown in Figure 20. The combined model fits the data within 10% of the measured value. All residuals are an order of magnitude smaller than the measured values and are within the measured error ranges. Similar to the unannealed device, the residuals have a periodic

structure. The increasing residuals in the negative voltage region indicate that outside the measured range the fitted FP model may not accurately describe the device. The flat band voltage is -0.06 V and the current at 0 V is 3.76×10^{-11}A. The linear FNT portion of the model shows a 0.125 eV potential for tunneling. The first FP model (FP1) begins at -0.13 V and continues to the -0.5 V, with a barrier potential of 0.1 eV and a parasitic resistance of $7\times10^{9}\,\Omega$. The second FP model (FP2) begins at -0.11 V and continues in a linear combination with FP1. FP2 has a potential barrier of 0.1 eV and a parasitic resistance of $1.6\times10^{9}\,\Omega$. The fitting parameters for the combined model for the annealed 14 nm h-BN (chip F) are shown in Table 8. The decreased flat band voltage is expected because the annealing process reduces the defect density of the h-BN/Si interface and reduces the trapped positive charge. The annealing process also reduces the defects within the substrate and the h-BN, which results in greater drift current because of the increased electron recombination lifetime. This is evident in the decrease of the FP parasitic resistances from the unannealed h-BN chip.

Table 8. Fitting parameters for annealed h-BN chip F.

Model	Parameter	Value	Units
	V_{FB}	-0.06	V
	I_{zero}	3.76×10^{-11}	A
FP 1	R_{pFP1}	7×10^{9}	Ω
	R_{pFP1} Begins	-0.13	V
	ϕ_{BFP1}	0.1	eV
FP 2	R_{pFP2}	1.6×10^{9}	Ω
	R_{pFP2} Begins	-0.11	V
	ϕ_{BFP2}	0.1	eV
Linear FNT	ϕ_{BLFNT}	0.125	eV
Non-linear FNT 1	R_{pFNT1}		Ω
	R_{pFNT1} Begins		V
	ϕ_{BFNT1}		eV
Non-linear FNT 2	R_{pFNT2}		Ω
	R_{pFNT2} Begins		V
	ϕ_{BFNT2}		eV

4.3 Gamma Irradiation Data Fitting

Chip E was irradiated with 33.1, 99.3 and 331 krad(Si) total accumulated doses with 3-7 days between each irradiation. The combined FP and FNT model were fitted to the gamma-irradiated 14 nm h-BN chip E shown in Figures 21-23. Every fifth measured value is displayed with a single standard deviation error bar. Figure 21 shows an increasing error in the measured current in the non-linear region. The linear FNT model dominates from 0.5 V to -0.13 V and the FP model dominates from -0.13 V to -0.5 V.

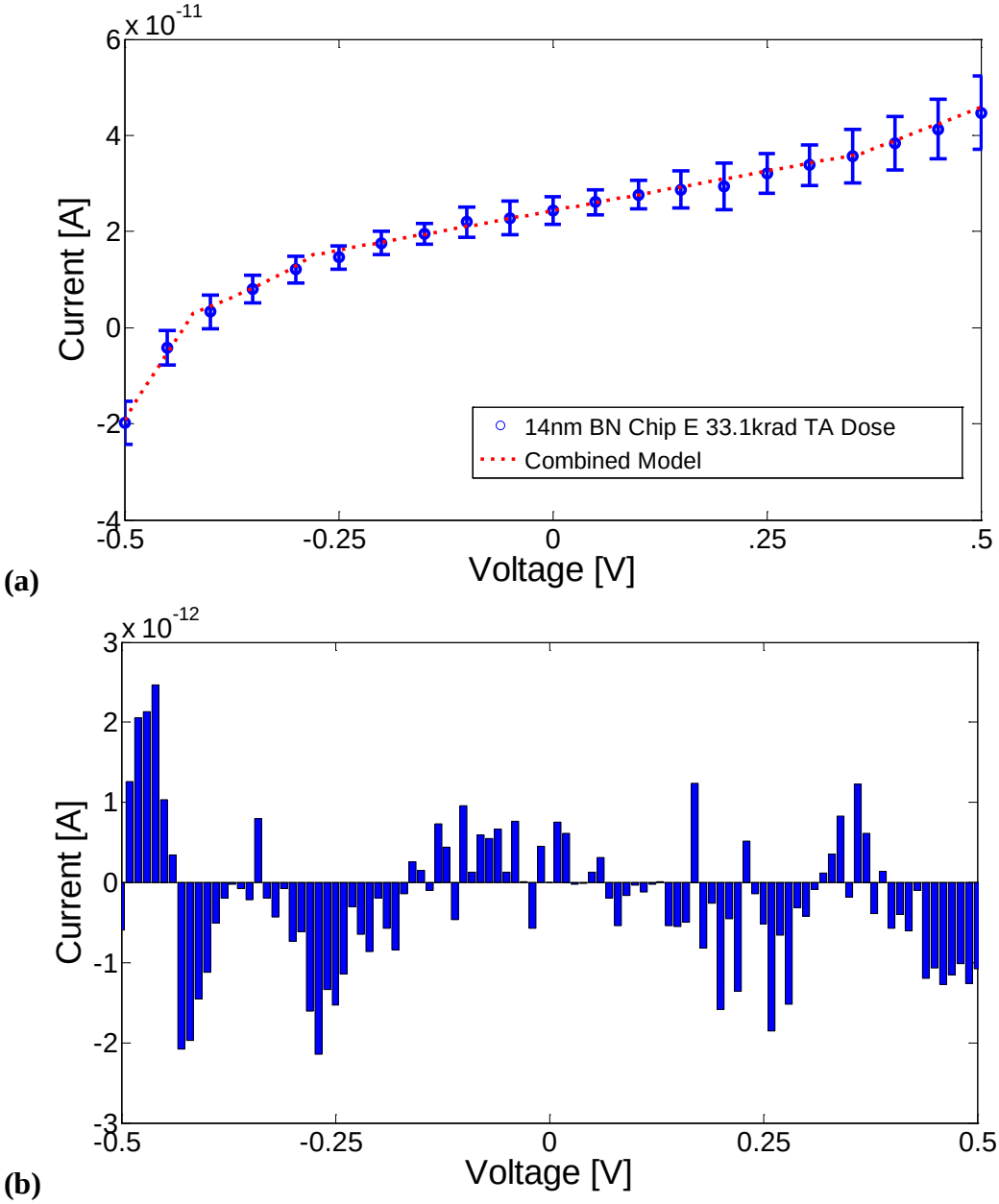

Figure 21. (a) Current as a function of voltage for h-BN chip E, with a total accumulated dose of 33.1 krad(Si), and combined FP, linear FNT, and non-linear FNT fitted models. (b) Associated residuals plot.

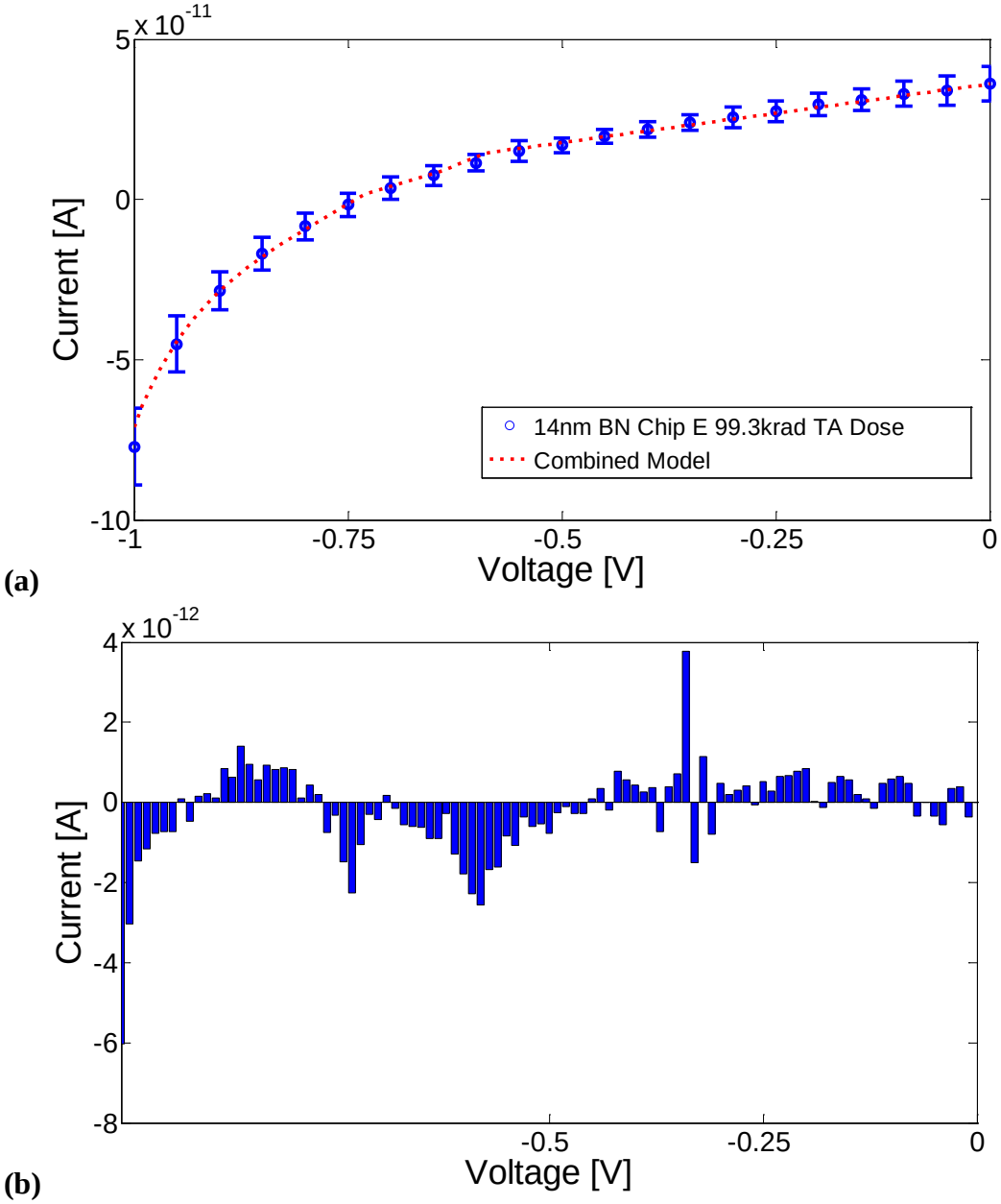

Figure 22. (a) Current as a function of voltage for h-BN chip E, with a total accumulated dose of 99.3 krad(Si), and combined FP, linear FNT, and non-linear FNT fitted models. (b) Associated residuals plot.

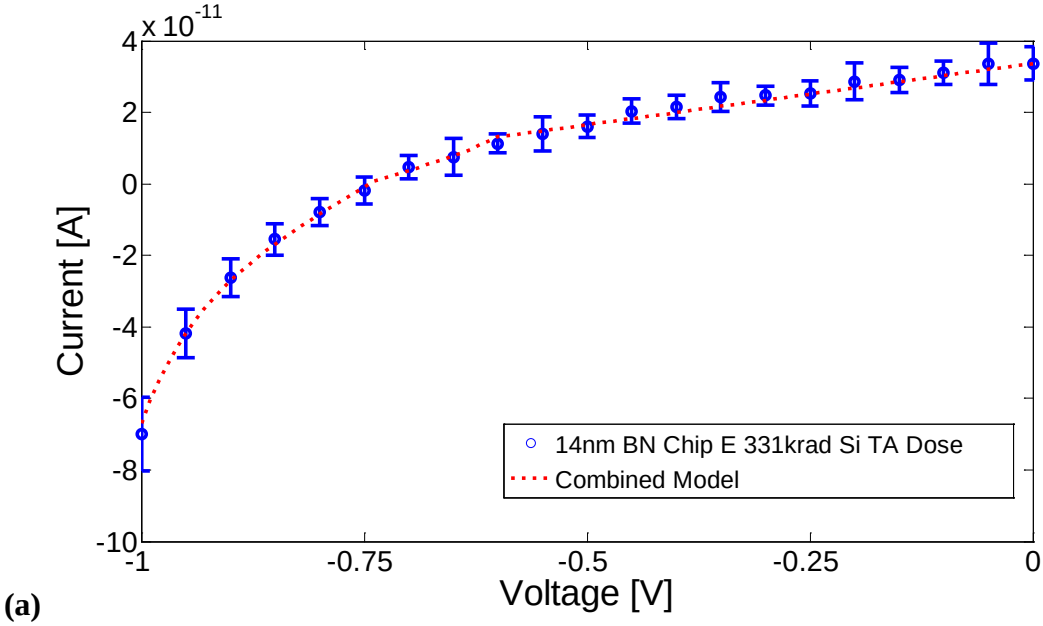

(a)

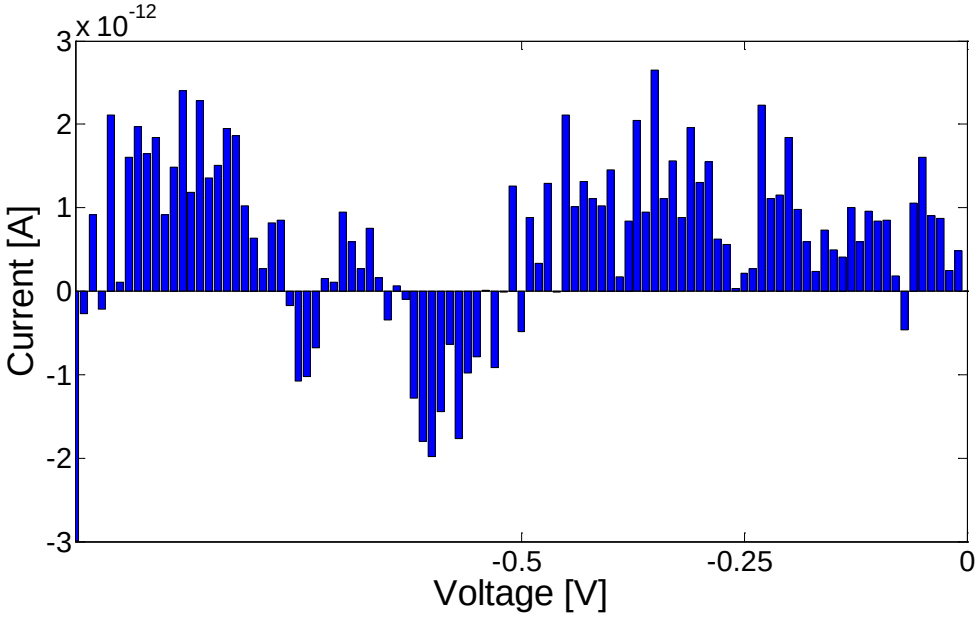

(b)

Figure 23. (a) Current as a function of voltage for h-BN chip E, with a total accumulated dose of 331 krad(Si), and combined FP, linear FNT, and non-linear FNT fitted models. (b) Associated residuals plot.

The residual plot between the measured and the combined model is shown in Figures 21-23. The combined model fits the data within 10% of the measured value.

All of the residuals are an order of magnitude smaller than the measured values, and are within the measured error ranges. The residuals do not show much structure and are due to random electronic noise, which does not contribute significantly to the measured values. The flat band voltage decreases from -0.28 V to -0.42, -0.73, and -0.74 V for 33.1, 99.3 and 331 krad (Si) total accumulated doses, respectively. Additionally, the current at 0 V changed from 2.2×10^{-11} to 2.4×10^{-11}, 3.6×10^{-11}, 3.6×10^{-11} A, respectively. The changes in the start of the FP dominate model corresponds to the negative voltage shifts of the flat band voltage. The barrier potential for the both the FP and FNT remain the same throughout the irradiations. Only the 331 krad(Si) total accumulated dose gamma irradiation had a slight decrease in the barrier potential for the FP 1, from 0.12 eV to 0.118 eV. In the FP1 region, the parasitic resistance was 2.5×10^{10} Ω pre- and post-irradiation. In the FP2 region, the parasitic resistance was 1.3×10^{10} Ω for the 99.3 and 331 krad(Si) doses. The parasitic resistance of the 33.1 krad(Si) dose in the FP2 region was 5.0×10^{9} Ω. The fitting parameters for the combined model for the gamma irradiated 14 nm h-BN (chip E) are shown in Table 9.

Table 9. Fitting parameters for h-BN chip E.

Model	Parameter	33.1 krad Si Total Accumulated Dose	99.3 krad Si Total Accumulated Dose	331 krad Si Total Accumulated Dose	Units
	V_{FB}	-0.42	-0.73	-0.74	V
	I_{zero}	2.4×10^{-11}	3.6×10^{-11}	3.6×10^{-11}	A
FP 1	R_{pFP1}	2.5×10^{10}	2.5×10^{10}	2.5×10^{10}	Ω
	R_{pFP1} Begins	-0.23	-0.54	-0.55	V
	ϕ_{BFP1}	0.12	0.12	0.118	eV
FP 2	R_{pFP2}	5.0×10^{9}	1.3×10^{10}	1.3×10^{10}	Ω
	R_{pFP2} Begins	-0.42	-0.54	-0.74	V
	ϕ_{BFP2}	0.12	0.12	0.12	eV
Linear FNT	ϕ_{BLFNT}	0.1343	0.1335	0.1340	eV
Non-linear FNT 1	R_{pFNT1}	2.8×10^{10}			Ω
	R_{pFNT1}	0.36			V
	ϕ_{BFNT1}	1.343			eV
Non-linear FNT 2	R_{pFNT2}				Ω
	R_{pFNT2}				V
	ϕ_{BFNT2}				eV

4.4 Neutron Irradiation Data Fitting

The combined FP and FNT model were fitted to the neutron irradiated 14 nm h-BN chip D shown in Figure 24. Every 5th measured value is displayed with a single standard deviation error bar. Figure 24 shows an increasing error in the measured current in the nonlinear regions with a significant increase in the FP dominated region below 0.75 V. The linear FNT model dominates from -0.25 V to 0.38 V, the nonlinear FNT model dominates from 0.38 V to 1 V and the FP model dominates from -0.25 V to -1.0 V.

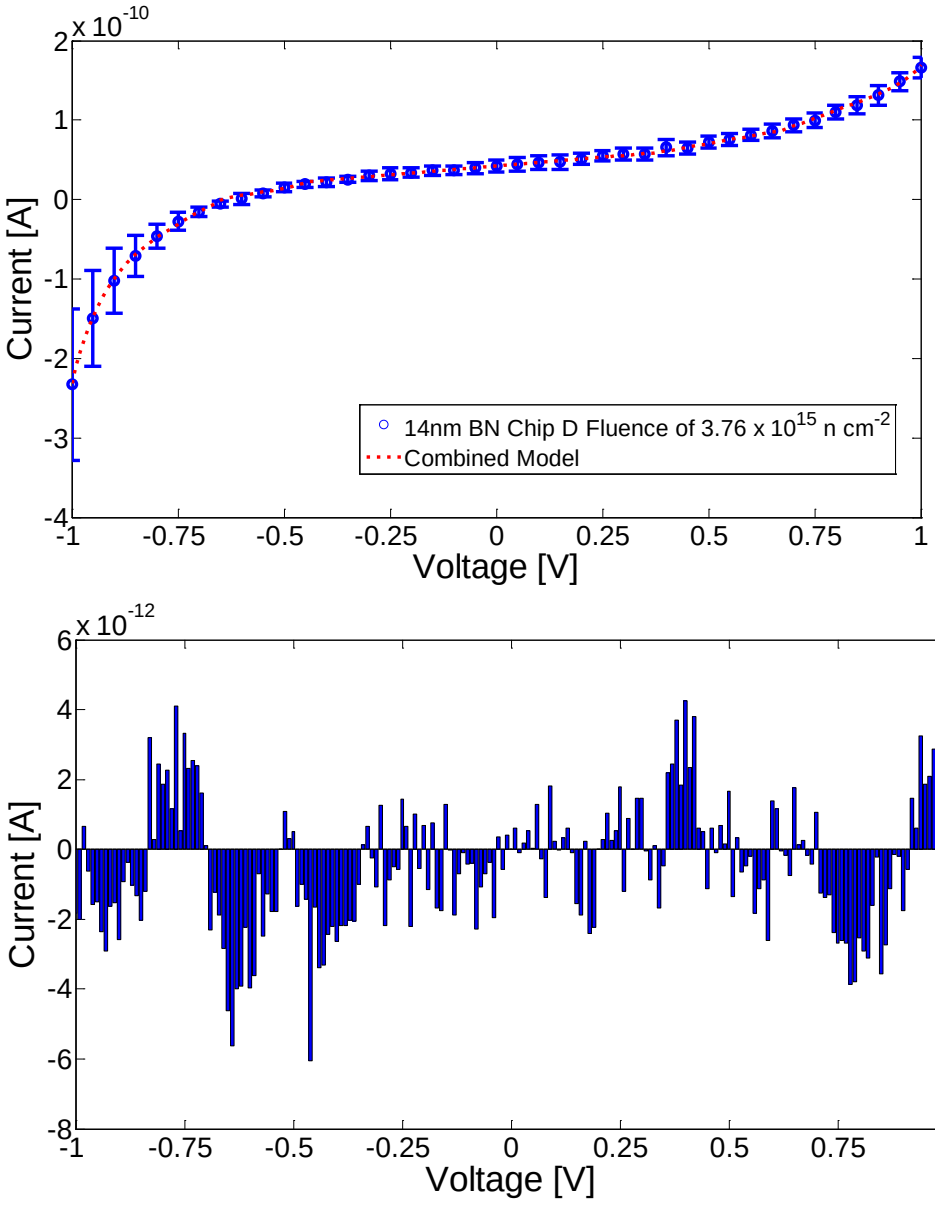

Figure 24. (a) Current as a function of voltage for h-BN chip D, following neutron irradiation, and combined FP, linear FNT, and non-linear FNT fitted models. (b) Associated residuals plot.

The residual plot between the measured and the combined model is shown in Figure 24. The combined model fits the data within 10% of the measured value. All of the residuals are two orders of magnitude smaller than the measured values and are

within the measured error ranges. The residuals do not show structure and appear to be random fluctuations. The flat band voltage is -0.62 V and the current at 0 V is 4.2×10^{-11} A. The linear FNT portion of the model shows a 0.132 eV potential for tunneling. The first FNT model (FNT1) begins at 0.38 V and continues to 1 V with a barrier potential of 1.12 eV and a parasitic resistance of $2.0\times10^{10}\,\Omega$. The second FNT model (FNT2) begins at 0.67 V and continues in a linear combination with FNT1. FNT2 has a potential barrier of 1.12 eV and a parasitic resistance of $1.0\times10^{10}\,\Omega$. The first FP model (FP1) begins at -0.25 V and continues to the -1 V with a barrier potential of 0.128 eV and a parasitic resistance of $2.5\times10^{10}\,\Omega$. The second FP model (FP2) begins at -0.64 V and continues in a linear combination with FP1. FP2 has a potential barrier of 0.128 eV and a parasitic resistance of $5.0\times10^{9}\,\Omega$. The fitting parameters for the combined model for the neutron irradiated 14 nm h-BN (chip D) are shown in Table 10.

Table 10. Fitting parameters for neutron irradiated 14 nm h-BN chip D.

Model	Parameter	Value	Units
	V_{FB}	-0.62	V
	I_{zero}	4.2×10^{-11}	A
FP 1	R_{pFP1}	2.5×10^{10}	Ω
	R_{pFP1} Begins	-0.25	V
	ϕ_{BFP1}	0.128	eV
FP 2	R_{pFP2}	5.0×10^{9}	Ω
	R_{pFP2} Begins	-0.64	V
	ϕ_{BFP2}	0.128	eV
Linear FNT	ϕ_{BLFNT}	0.132	eV
Non-linear FNT 1	R_{pFNT1}	2.0×10^{10}	Ω
	R_{pFNT1} Begins	0.38	V
	ϕ_{BFNT1}	1.12	eV
Non-linear FNT 2	R_{pFNT2}	1.0×10^{10}	Ω
	R_{pFNT2} Begins	0.67	V
	ϕ_{BFNT2}	1.12	eV

The combined FP and FNT model were fitted to the neutron irradiated annealed 14 nm h-BN chip F shown in Figure 25. Every 5^{th} measured value is displayed with a single standard deviation error bar. Figure 25 shows an increasing error in the measured current in the nonlinear regions with a significant increase in both the FP and FNT dominated region below -0.75 V and above 0.6 V respectively. The linear FNT model dominates from -0.41 V to 0.38 V, the nonlinear FNT model dominates from 0.38 V to 1 V and the FP model dominates from -0.41 V to -1.0 V.

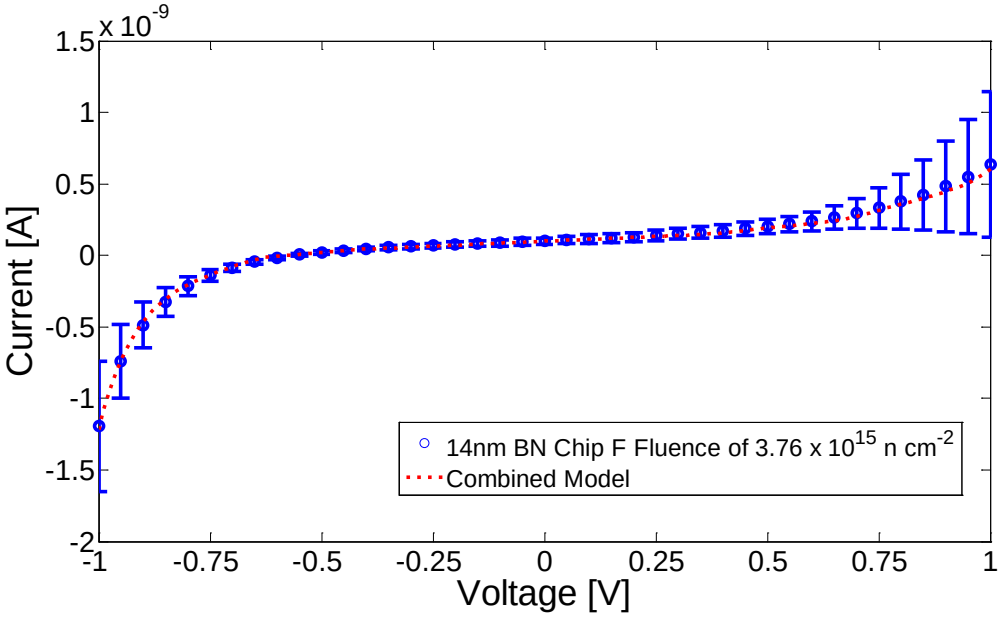

(a)

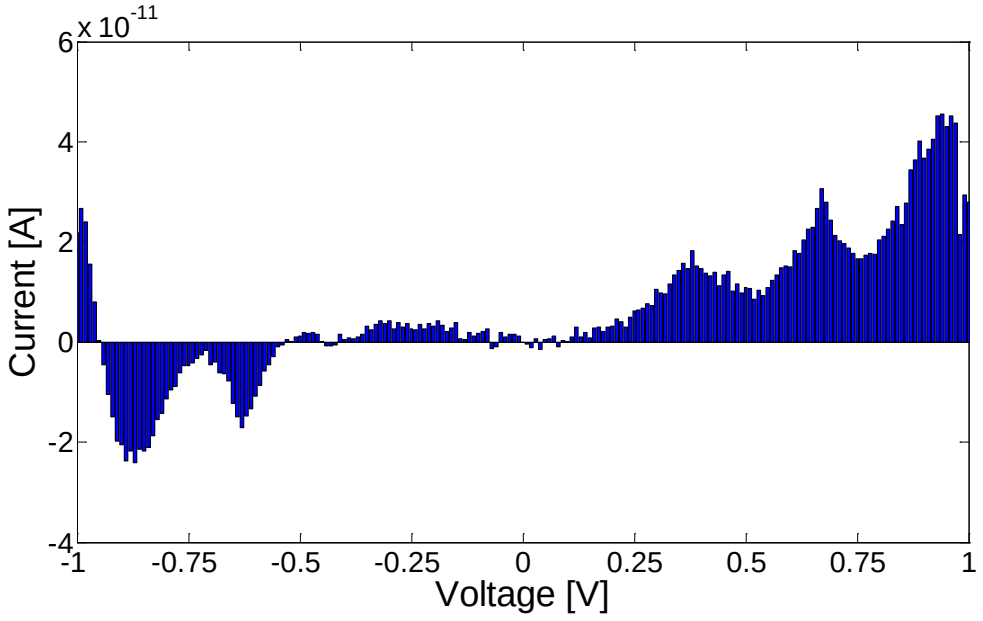

(b)

Figure 25. (a) Current as a function of voltage for annealed h-BN chip F, following neutron irradiation, and combined FP, linear FNT, and non-linear FNT fitted models and (b) associated residuals plot.

The residual plot between the measured and the combined model is shown in Figure 25. The combined model fits the data within 10% of the measured value. All of the residuals are two orders of magnitude smaller than the measured values and are within the measured error ranges. The residuals do show the measured values are slightly higher in the positive voltage region. The flat band voltage is -0.56 V and the current at 0 V is 9.9×10^{-11} A. The linear FNT portion of the model shows a 0.124 eV potential for tunneling. The first FNT model (FNT1) begins at 0.38 V and continues to the 1 V with a barrier potential of 1.06 eV and a parasitic resistance of $5.0\times10^{9}\ \Omega$. The second FNT model (FNT2) begins at 0.67 V and continues in a linear combination with FNT1. FNT2 has a potential barrier of 0.915 eV and a parasitic resistance of $2.0\times10^{9}\ \Omega$. The first FP model (FP1) begins at -0.41 V and continues to the -1 V with a barrier potential of 0.1 eV and a parasitic resistance of $8.0\times10^{9}\ \Omega$. The second FP model (FP2) begins at -0.63 V and continues in a linear combination with FP1. FP2 has a potential barrier of 0.1 eV and a parasitic resistance of $1.6\times10^{9}\ \Omega$. The fitting parameters for the combined model for the neutron irradiated annealed 14 nm h-BN (chip F) are shown in Table 11.

Table 11. Fitting parameters for neutron irradiated 14nm annealed h-BN chip F.

Model	Parameter	Value	Units
	V_{FB}	-0.56	V
	I_{zero}	9.9×10^{-11}	A
FP 1	R_{pFP1}	8×10^{9}	Ω
	R_{pFP1} Begins	-0.41	V
	ϕ_{BFP1}	0.1	eV
FP 2	R_{pFP2}	1.6×10^{9}	Ω
	R_{pFP2} Begins	-0.63	V
	ϕ_{BFP2}	0.1	eV
Linear FNT	ϕ_{BLFNT}	0.124	eV
Non-linear FNT 1	R_{pFNT1}	5.0×10^{9}	Ω
	R_{pFNT1} Begins	0.38	V
	ϕ_{BFNT1}	1.06	eV
Non-linear FNT 2	R_{pFNT2}	2.0×10^{9}	Ω
	R_{pFNT2} Begins	0.67	V
	ϕ_{BFNT2}	0.915	eV

4.5 Changes in Device Characteristics from Irradiations

Changes in *C-V characteristics following irradiation*

The gamma irradiation of chip E, h-BN, resulted in no significant changes in the measured capacitance. Both the pre- and post-irradiation values for the capacitance were within one sigma error from each other. Additionally, neutron irradiation had no significant effect on the capacitance of chip D, 14 nm h-BN, and chip F, annealed h-BN.

The Si chip capacitance decreased from 237 pF to 2.5 pF following neutron irradiation, as shown in Figure 26. Neutron irradiation resulted in displacement damage to the Si in the form of defect clusters from the $n + {}^{10}B$ reaction. The resulting Li and alpha particles are the primary knock-on atoms (PKA) with sufficient energy to cause thousands of point defects within the range of the particle. The large amount of damage

to the Si would cause the conductivity of the silicon to decrease, and subsequently, the capacitance of the silicon to decrease as well.

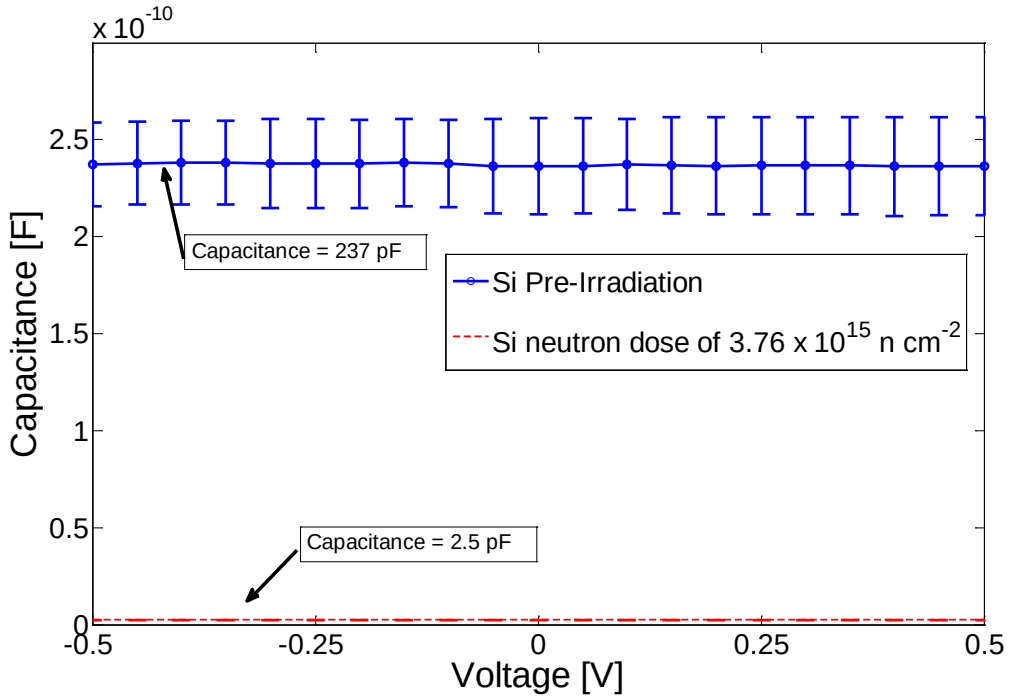

Figure 26. Capacitance as a function of voltage for the Si device before and after neutron irradiation.

Changes in Flat Band Voltage Following Irradiation

The gamma irradiation of the silicon chip and the BN chip E caused a negative shift in the flat band voltage, shown in Figures 27 and 28. The negative shift corresponds to positive charge trapping at the interface of the SiO_2/Si and the h-BN/Si. The gamma radiation causes charge generation within the device and the charge is being trapped at interface states between the h-BN/Si interface.

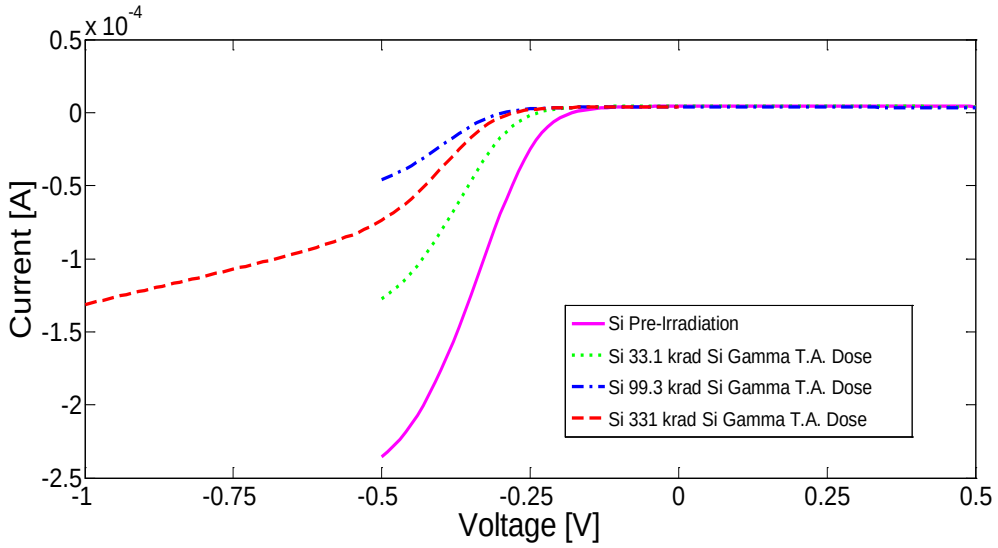

(a)

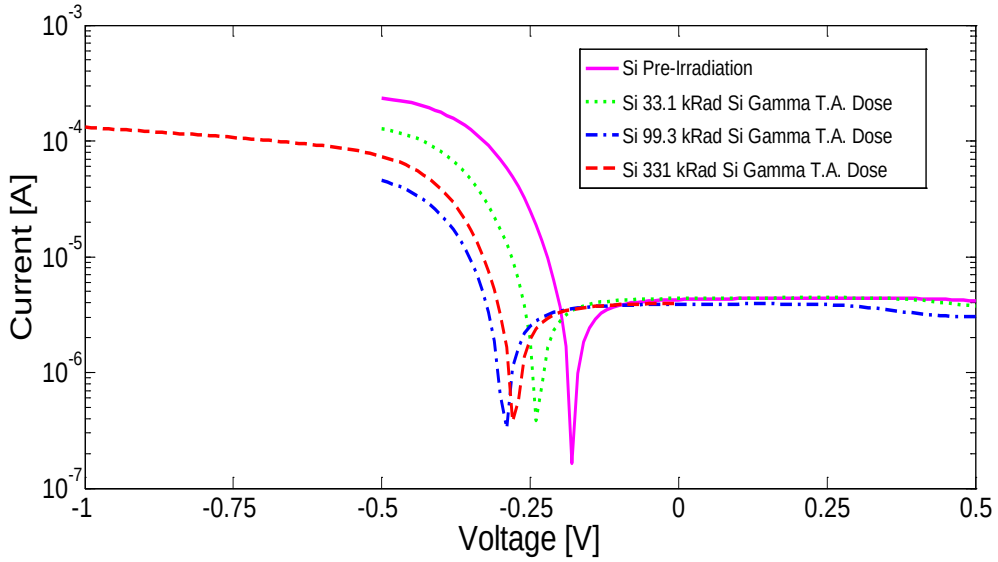

(b)

Figure 27. Current as a function of voltage for the Si device before and following gamma irradiation, plotted on (a) linear-linear and (b) logarithmic-linear scales.

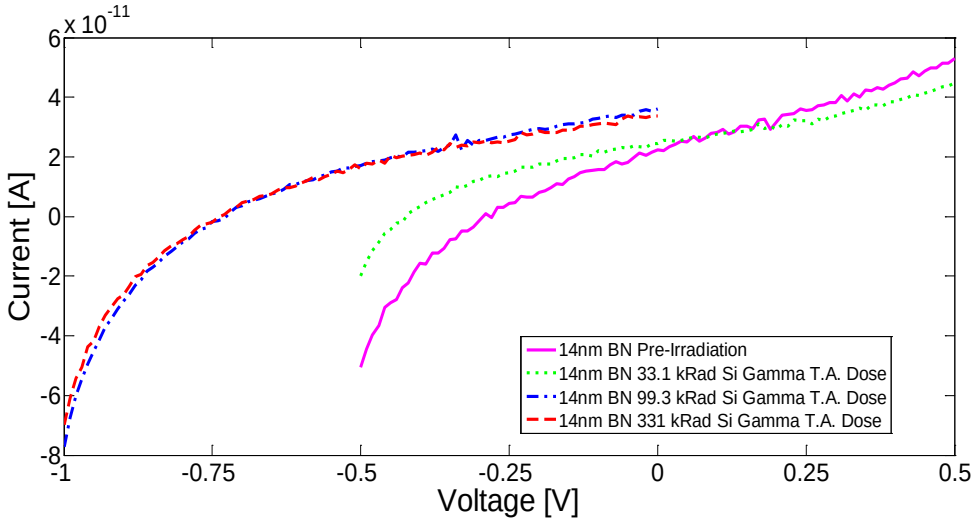

(a)

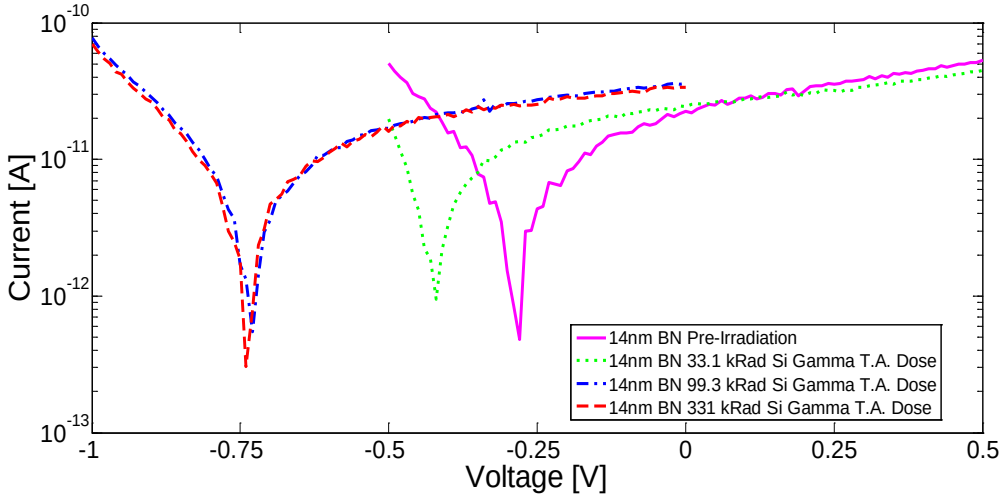

(b)

Figure 28. Current as a function of voltage for h-BN chip E before and following gamma irradiations, plotted on (a) linear-linear and (b) logarithmic-linear scales.

The 14 nm h-BN and the silicon devices exhibit a flat band shift saturation point, shown in Figure 29. The silicon has a shift from -0.18 to -0.29 V from the gamma irradiation. The 14 nm h-BN has a maximum shift from -0.28 to -0.74 V from the gamma

irradiation. The shift in flat band voltage for the 14 nm h-BN device is larger than that of the Si device because it is an insulator, and the structure of the BN allows for more charge trapping at the interface because of the lattice mismatch between the BN hexagonal structure and silicon.

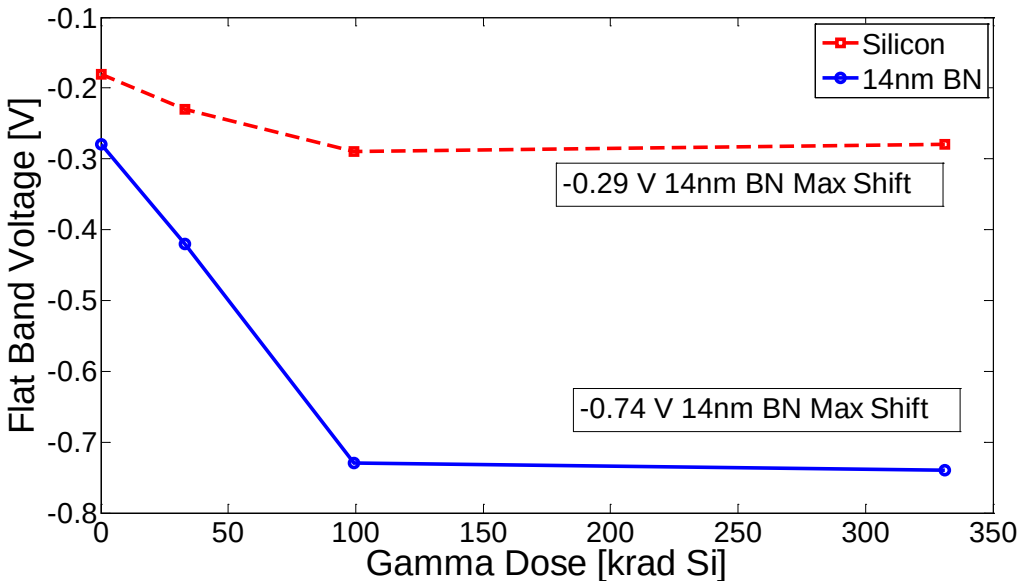

Figure 29. The change in flat band voltage as a function of total accumulated dose for both 14 nm BN chip E and p+ Si.

The neutron irradiation of the 14 nm BN (chip D) resulted in a negative shift in the flat band voltage, but not as large of a shift as was observed for the device exposed to gamma irradiation. The gamma radiation resulted in a negative shift of -0.46 V, compared to a shift of -0.34 V for the h-BN device following neutron irradiation. The *I-V* curves for Si, h-BN and annealed h-BN are shown in Figures 30 and 31.

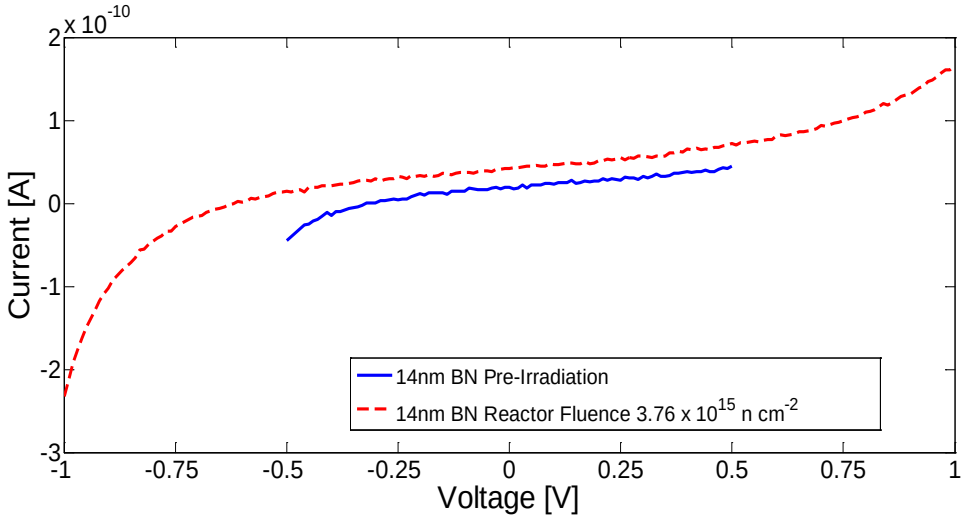

(a)

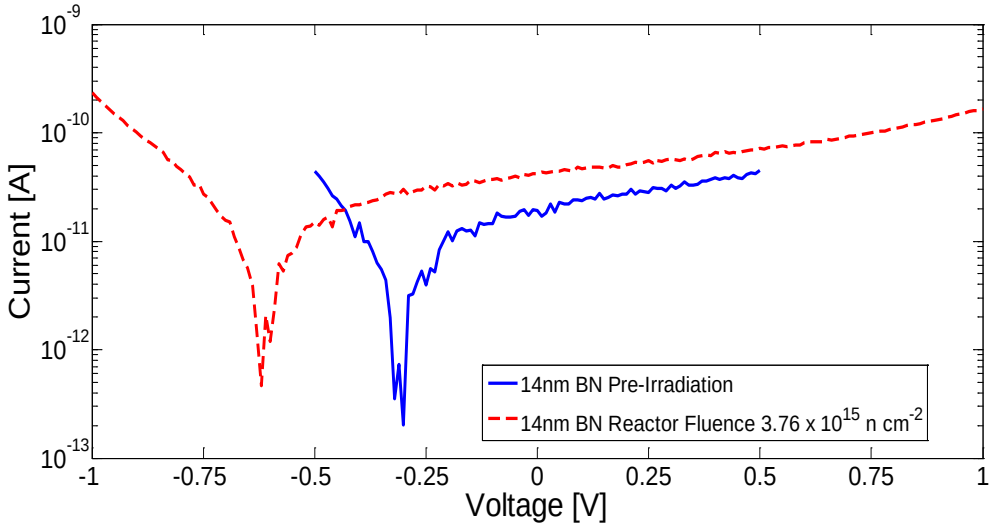

(b)

Figure 30. Current as a function of voltage for hBN chip D before and following neutron irradiation, plotted on (a) linear-linear and (b) logarithmic-linear scales.

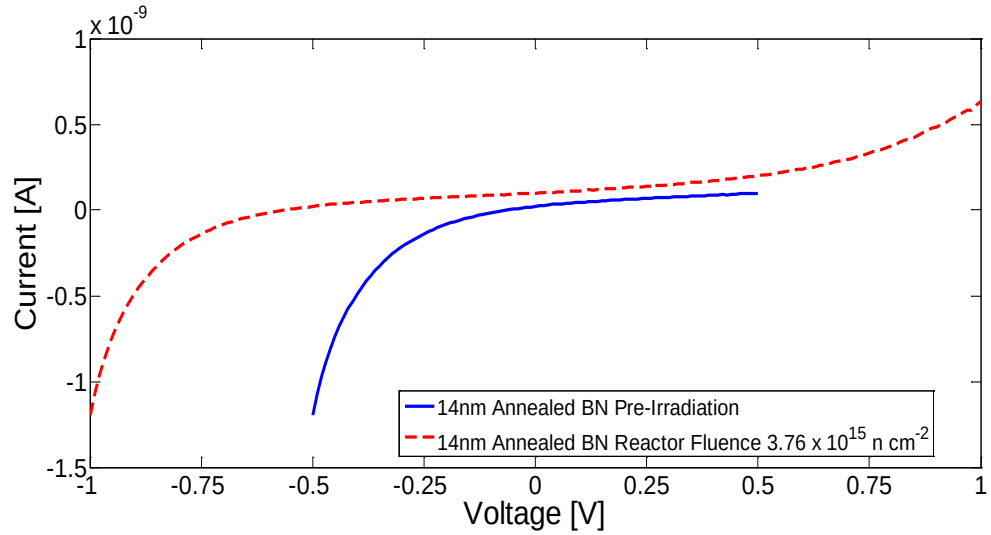

(a)

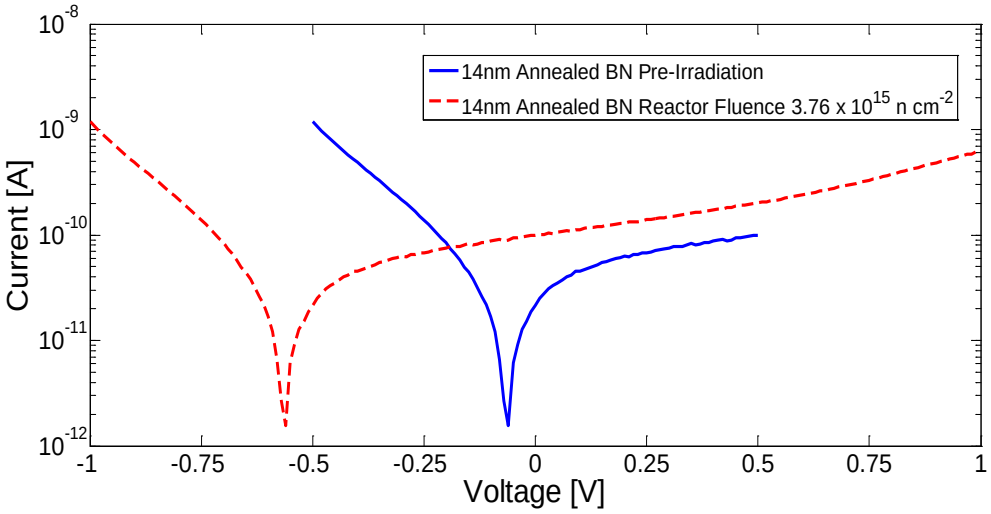

(b)

Figure 31. Current as a function of voltage for annealed h-BN chip F before and following neutron irradiation, plotted on (a) linear-linear and (b) logarithmic-linear scales .

The 14 nm h-BN and the 14 nm annealed h-BN show a slight increase in current magnitude following neutron irradiation. This increase corresponds to an increased leakage current through the h-BN layer from neutron-induced displacement damage. The

silicon device exhibits a positive shift in the flat band voltage of 0.1 V. Additionally, the current magnitude in the silicon device decreased by an order of magnitude, and the voltage dependence of the current decreased significantly, as well. These parameters all correspond to high levels of defect cluster damage that degrades the conductivity of the silicon. This results in a much higher resistance in the silicon, a smaller slope in the *I-V* curve, and a decrease in current magnitude. The positive voltage shift in the silicon device indicates negative trapped charge buildup at the interface. The neutrons react with the ^{10}B in the h-BN and the substrate, causing vacancy formation and unsatisfied bonds in h-BN and Si lattice.

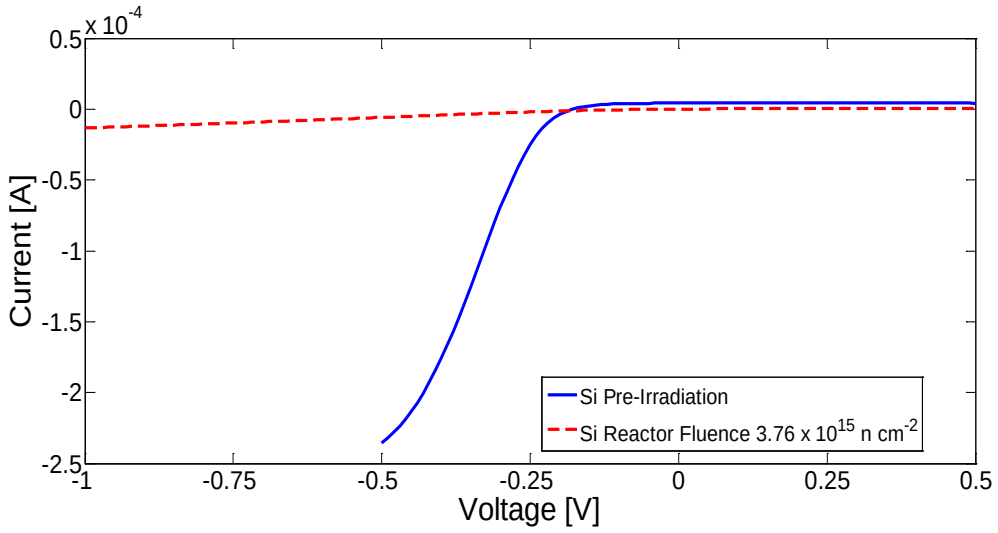

(a)

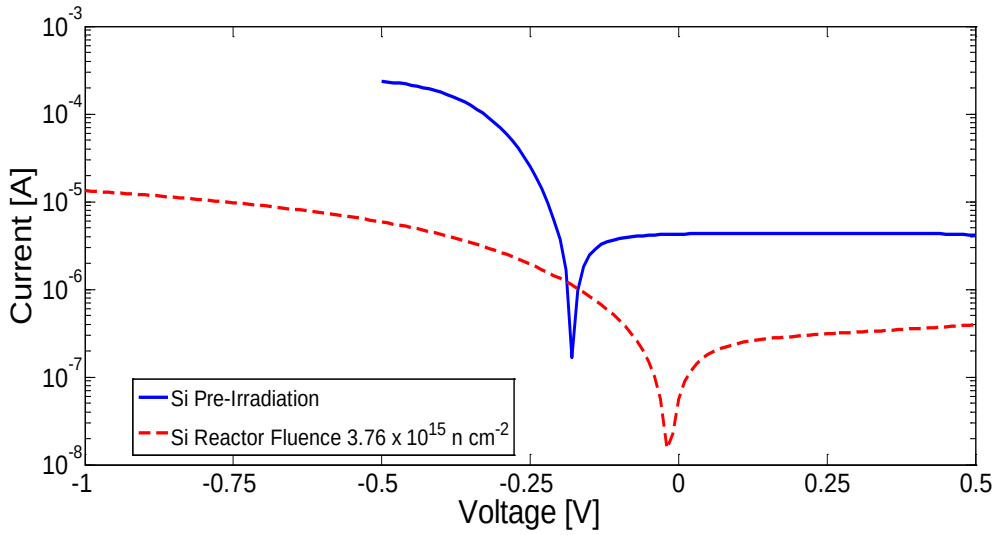

(b)

Figure 32. Current as a function of voltage for p+ Si before and following neutron irradiation, plotted on (a) linear-linear and (b) logarithmic-linear scales.

Changes in Barrier Potential following irradiation.

Gamma irradiation had no significant effect on the barrier potential for either FNT or FP emission. This implies that gamma radiation did not change the structure of the devices through displacement damage, and only increased the trapped positive charge at

the interface of the devices, resulting in a negative *I-V* curve shift. Neutron irradiation caused no change in the barrier potential for the linear FNT model, and only a slight increase in the barrier potential for the FP model. There was a decrease of 0.19 eV in the potential for the nonlinear FNT model for 14 nm h-BN chip D. The defects created by neutron irradiation create intermediate energy states between the valence band and conduction band, which lowers the barrier for an electron to tunnel by TAT.

4.6 Summary of results

The gamma and neutron irradiation of h-BN produced no significant changes to the measured capacitance. Both the pre- and post-irradiation values for the capacitance were within one sigma error from each other. The capacitance of the silicon decreased from 237 pF to 2.5 pF following neutron irradiation. Neutron irradiation caused severe displacement damage to the silicon in the form of defect clusters from the $n + {}^{10}B$ reaction. The large amount of damage to the Si caused a decrease in both the conductivity and capacitance of the silicon.

Gamma irradiation of the silicon and the h-BN device resulted in a negative shift in the flat band voltage, as noted in Table 12. The silicon flat band voltage shifted from -0.18 V to -0.29 V, while the h-BN flat band voltage shift was from -0.28 V to -0.74 V. Neutron irradiation of the h-BN caused the flat band voltage to shift negatively, but not as great as that resulting from gamma irradiation, even though the device received a larger gamma radiation dose in the AIF during neutron irradiation. Gamma radiation shifted the flat band voltage by -0.46 V for the BN and -0.11 V for Si, as compared to the neutron radiation shifted -0.34 V for h-BN and 0.1 V.

Table 12. Table of all fitted parameters and changes from pre-gamma irradiation values.

Model	Parameter	Pre-Irradiation Values	33.1 krad Si TA Dose Change in Values	99.3 krad Si TA Dose Change in Values	331 krad Si TA Dose Change in Values	Units
	V_{FB}	-0.28	-0.14	-0.45	-0.46	V
	I_{zero}	2.2×10^{-11}	1.9×10^{-12}	1.37×10^{-11}	1.12×10^{-11}	A
FP 1	R_{pFP1}	2.5×10^{10}	0	0	0	Ω
	R_{pFP1} Begins	-0.11	-0.12	-0.43	-0.44	V
	ϕ_{BFP1}	0.12	0	0	-0.002	eV
FP 2	R_{pFP2}	9.1×10^{9}	-4.1×10^{9}	3.9×10^{9}	3.9×10^{9}	Ω
	R_{pFP2} Begins	-0.37	-0.05	-0.36	-0.37	V
	ϕ_{BFP2}	0.12	0.0043	0.0035	0.004	eV
Linear FNT	ϕ_{BLFNT}	0.13	0	0	0	eV
Non-linear	R_{pFNT1}					Ω
	R_{pFNT1} Begins					V
	ϕ_{BFNT1}					eV
Non-linear	R_{pFNT2}					Ω
	R_{pFNT2} Begins					V
	ϕ_{BFNT2}					eV

The h-BN and the annealed h-BN exhibit a slight increase in the current magnitude following neutron irradiation. The increase corresponds to an increased leakage current through the h-BN layer from neutron damage. The silicon chip has a positive change in the flat band voltage of 0.1 V, which makes the flat band voltage of the silicon nearly zero after the irradiation. The current in the silicon decreased by an order of magnitude and the *I-V* curve flattened. The positive voltage shift in the Si chip would indicate negative charge buildup at the interface. The neutrons react with the ^{10}B in the h-BN and the substrate. The reaction causes a vacancy defect and unsatisfied bonds in h-BN and Si lattice.

The gamma irradiation resulted in no significant changes in the barrier potential for either FNT or FP emission. The gamma radiation did not change the structure of the

devices through displacement damage and only increased the trapped positive charge at the interfaces of the devices. The neutron irradiation caused no change in the barrier potential for the linear FNT model and only a slight increase in the barrier potential for the FP model. There was a decrease of 0.19 eV in the potential for the nonlinear FNT model for 14 nm h-BN noted in Table 13. The defects generated by the neutron damage could lower the barrier for an electron to tunnel by TAT, allowing intermediate energy states between the valence band and the conduction band, where the electron could tunnel into to the trap and then the conduction band.

Table 13. Table of all fitted parameters and changes from pre-neutron irradiation values.

Model	Parameter	Pre-Irradiation Values Chip D	Chip D $3.76x10^{15}$ n cm^{-2} fluence Change in Values	Pre-Irradiation Values Chip F	Chip F $3.76x10^{15}$ n cm^{-2} fluence Change in Values	Units
	V_{FB}	-0.62	-0.34	-0.06	-0.5	V
	I_{zero}	4.2×10^{-11}	1.9×10^{-11}	3.7×10^{-11}	6.1×10^{-11}	A
FP 1	R_{pFP1}	2.5×10^{10}	0	7×10^{9}	1.0×10^{9}	Ω
	R_{pFP1} Begins	-0.25	-0.26	-0.13	-0.54	V
	ϕ_{BFP1}	0.128	0.013	0.1	0	eV
FP 2	R_{pFP2}	5.0×10^{9}	-4.1×10^{9}	1.6×10^{9}	0	Ω
	R_{pFP2} Begins	-0.64	-0.29	-0.11	-0.52	V
	ϕ_{BFP2}	0.128	0.018	0.1	0	eV
Linear FNT	ϕ_{BLFNT}	0.132	0.001	0.125	-0.001	eV
Non-linear FNT1	R_{pFNT1}	2.0×10^{10}	-8.0×10^{9}			Ω
	R_{pFNT1} Begins	0.38	0.02			V
	ϕ_{BFNT1}	1.12	-0.19			eV
Non-linear FNT2	R_{pFNT2}	10^{10}				Ω
	R_{pFNT2} Begins	0.67				V
	ϕ_{BFNT2}					eV

V. Conclusions and Recommendations

5.1 Conclusions of Research

Pre-irradiation *I-V* and *C-V* data are consistent with FP and FNT tunneling models. The analytical models provide a very good fit to the measured pre- and post-irradiation currents from -1 to 1 V. It has been demonstrated that the Schottky emission did not fit the measured data. Linear FNT fit the data well when the applied potential was very small. The nonlinear FNT fit well in the positive voltage region and FP emission fit well in the negative voltage region.

The potential barrier, ϕ, is an extremely sensitive parameter when fitting to experimental currents. Varying the potential barrier by 0.01 eV in all models used in this research will result in significant current changes. Its impact on the results makes it an important parameter to measure in future research. The linear combination of multiple FP or FNT models suggests a higher fidelity model may be necessary to accurately describe the behavior of the current characteristics outside of the current data range.

Gamma irradiation exposure at the doses received from the cobalt-60 source does not result in displacement damage to the device. Gamma irradiation results in a negative flat band voltage shift that saturates based on the dimensions of the MIS device. Neutron irradiation causes permanent damage by creating defects within the substrate and at the h-BN/Si interface.

When designing a device with graphene on silicon, the radiation response is largely due to the interface characteristics. The h-BN is more radiation resistant to neutron radiation than silicon. There was not enough independent data generated in this

research to conclude that increased defect density was responsible for the increased current after neutron irradiation. Further experimentation, which could be obtained by using other techniques such as Raman spectroscopy or photoluminescence spectroscopy would be required.

5.2 Recommendations for Future Research

The use of *I-V* and *C-V* measurements provides a method to determine the radiation response of h-BN/Si MIS devices. Further characterization and analysis can be achieved by including admittance measurements. Admittance measurements of the devices will give an accurate conductivity measurement of the h-BN film. Additionally temperature dependent current measurements will allow the separation of specific defect mechanisms by their activation energy. Te effect of neutron spectra and flux should be investigated, which will enable the identification of which energy is causing specific damage and if there is a threshold. *In-situ* measurements for both gamma and neutron irradiations would allow the time dependent response of the devices to be quantified. These additional measurements would enable the further identification of damage mechanisms and their effect.

The mechanisms proposed for increased current and increased trap density following irradiation can be explored further by irradiating MIS devices of varying dimensions and measuring trap density using spectroscopic techniques. Studying the lattice structure and the h-BN/Si interface with Raman or optical techniques would provide further insight into the damage mechanisms and quantify damage parameters.

Bibliography

[1] M. Schieber, M. Roth, A. Zuck and O. Khakhan, "Polycrystalline BN and LiF Based Semiconductor Alpha Particle and Neutron Detectors," *IEEE Nuclear Science Symposium Conference Record,* pp. 3728-3731, 2006.

[2] L. Song, "Large Scale Growth and Characterization of Atomic Hexagonal Boron Bitride Layers," *Nano Letters,* pp. 6-12, 2010.

[3] O. Ozdemir, "Instability phenomenon orginated from the disorded layer of plasma-deposited BN film/c-Si Interface assessed through the MIS structure by admittance measurement," *Semiconductor Science Technology,* vol. 23, 2008.

[4] C. Steinborn, M. Herrmann, U. Keitel and A. Schonecker, "Correlation between microstructure and electrical resistivity of hexagonal boron nitride ceramics," *Journal of the European Ceramic Society,* vol. 33, pp. 1225-1235, 2013.

[5] G.-H. Lee, Y.-J. Yu, C. Lee, C. Dean and K. L. Shepard, "Electron tunneling through atomically flat and ultrathin hexagonal boron nitride," *Applied physics letters,* vol. 99, 2011.

[6] T. Zhang, "Permittivity and its Temperature Dependence on Hexagonal Structure BN Dominated by the Local Electric Field," *Chinese Physical Society,* vol. 21, no. 7, 2012.

[7] M. Snure, Q. Paduano, M. Hamilton, J. Shoaf and J. M. Mann, "Optical Characterization of Nanocrystalline Boron Nitride Thin Films Grown by Atomic Layer Deposition," *Thin Solid Films,* no. 571, pp. 51-55, 2014.

[8] H. X. Chen, X. G. Zhao, Z. J. Ma, Y. Li and S. Y. Ma, "The Effects of Microstructure on I-V Properties of Si/SiO2 Film," *Nanotech,* vol. 1, pp. 356-359, 2009.

[9] M. Brotzmann, H.-G. Gehrke and U. Vetter, "Modeling the diode characteristics of boron nitride/silicon carbide heterojunctions," *Applied Physics Letters,* vol. 97, 2010.

[10] M. J. Hanna, H. Zhao and J. C. Lee, "Poole Frenkel current and Schottky emission in SiN gate dielectric in AlGaN/GaN metal insulator semiconductor heterostructure field effect transistors," *Applied Physics Letters,* vol. 101, 2012.

[11] L. Britnell, R. V. Gorbachev and R. Jalil, "Electron Tunneling through Ultrathin Boron Nitride Crystalline Barriers," *Nano Letters,* vol. 12, pp. 1707-1710, 2012.

[12] S. Ristic, A. Prijic and Z. Prijic, "Dependence of Static Dielectric Constant of Silicon on Resistivity at Room Temperature," *Serbian Journal of Electrical Engineering,* vol. 1, no. 2, pp. 237-247, 2004.

[13] "Gate Dielectric Capacitance-Voltage Characterization Using Model 4200 Semiconductor Characterization System.," in *Keithley Application Note Series, Number 2239,* 2006.

[14] Engineering Web Services, "The Ohio State University Reactor Lab," [Online]. Available: https://reactor.osu.edu/. [Accessed 10 October 2014].

[15] B. Buyuk, A. B. Tugrul and A. O. Addemir, "Gamma Attenuation Behavior of h-BN and h-BN-TiB2 Composites," in *Proceedings of the 3rd Internation Congress,* Antalya, Turkey, 2013.

[16] J. Uher, S. Pospisil and V. Linhart, "Efficiency of composite boron nitride neutron detectors in comparison with helium-3 detectors," *Applied Physics Letters,* vol. 90, 2007.

[17] "Space Radiation and its Effects on EEE Components," EPFL Space Center, 2009.

[18] Device Characterization with the Keithley Model 4200-SCS Chararcterization System., Keithley Instraments Inc, 2006.

[19] C. X. Zhang, B. Wang and G. X. Duan, "Total ionizing dose effects on encapulated graphene-hBN devices".

[20] C. M. Orofeo, S. Suzuki and H. Hibino, "Ultrathin CVD-grown Hexagonal Boron Nitride as a High-quality Dielectric for Tunneling Devices on Rigid and Flexible Sunstrates," *Journal of Physical Chemistry C,* 2014.

[21] Z. Li, "Radiation Hardness/Tolerance of Si Sensors/Detectors for Nuclear and High Energy Physics Experiments," Brookhaven National Laboratory, NY.

REPORT DOCUMENTATION PAGE

Form Approved
OMB No. 0704-0188

PLEASE DO NOT RETURN YOUR FORM TO THE ABOVE ADDRESS.

1. REPORT DATE *(DD-MM-YYYY)*	2. REPORT TYPE	3. DATES COVERED *(From - To)*
26-03-2015	Master's Thesis	Sept 2013-March 2015

4. TITLE AND SUBTITLE

Ionizing and Non-ionizing Radiation Effects in Thin Layer Hexagonal Boron Nitride

5a. CONTRACT NUMBER

5b. GRANT NUMBER

F4F5AR3224A003

5c. PROGRAM ELEMENT NUMBER

6. AUTHOR(S)

Barnett, Brian L, MAJ, Army

5d. PROJECT NUMBER

5e. TASK NUMBER

5f. WORK UNIT NUMBER

7. PERFORMING ORGANIZATION NAME(S) AND ADDRESS(ES)

Air Force Institute of Technology
Graduate School of Engineering and Management (AFIT/EN)
2950 Hobson Way
Wright-Patterson AFB OH 45433-7765

8. PERFORMING ORGANIZATION REPORT NUMBER

AFIT-ENP-MS-15-M-099

9. SPONSORING/MONITORING AGENCY NAME(S) AND ADDRESS(ES)

Nuclear Effects Analysis Division
Air Force Nuclear Weapons Center
8601 Frost Avenue SE
Kirtland AFB NM 87117
Col Mark Suriano USAF AFNWC/NCA, mark.suriano@us.af.mil

10. SPONSOR/MONITOR'S ACRONYM(S)

11. SPONSOR/MONITOR'S REPORT NUMBER(S)

12. DISTRIBUTION/AVAILABILITY STATEMENT

Distribution Statement A. Approved for Public Release; Distribution Unlimited

13. SUPPLEMENTARY NOTES

This material is declared a work of the U.S. Government and is not subject to copyright protection in the United States.

14. ABSTRACT

The radiation response of 14nm h-BN/Si metal insulator semiconductor (MIS) devices was investigated using current-voltage and capacitance-voltage measurements indicating Frenkel Poole (FP) and Fowler-Nordheim tunneling (FNT) are the primary current mechanisms before and after irradiation. The data were fit to a composite model of FP and FNT currents. Irradiations to 33.1, 99.3, and 331 krad(Si) from a cobalt-60 source causes a negative voltage shift to the current-voltage measurements of -0.14, -0.45, and -0.46 V respectively. The negative shift indicates radiation induced production of positive space charge at the h-BN/Si interface. No device characteristic changes were observed following gamma irradiation. Fitting the model to data collected after neutron irradiation at a fluence of 3.76x1015 n/cm2 indicated no change in the barrier potential for the linear FNT model and a 0.013 eV increase in the barrier potential for the FP model. There was a decrease of 0.19 eV in the tunneling potential for the non-linear FNT model. Defects generated by the neutron damage increased currents by increasing trap assisted tunneling (TAT).

15. SUBJECT TERMS

Hexagonal Boron Nitride, Metal Insulator Semiconductor, Trap Assisted Tunneling

16. SECURITY CLASSIFICATION OF:			17. LIMITATION OF ABSTRACT	18. NUMBER OF PAGES	19a. NAME OF RESPONSIBLE PERSON
a. REPORT	b. ABSTRACT	c. THIS PAGE			Dr. James C. Petrosky, AFIT/ENP
U	U	U	UU	83	19b. TELEPHONE NUMBER *(Include area code)* (937) 255-3636 x4563 James.Petrosky@afit.edu

Reset